Proceedings Book Series -PBS-

10th International Conference on Green Energy & Environmental Engineering

-GEEE-

Editor : Dr. Ahmed Rhif (Tunisia)

CNPSI

Centre National de la Promotion Scientifique et de L'innovation

Proceedings Book Series -PBS-

10th International Conference on Green Energy & Environmental Engineering

-GEEE-

PBS-Vol. 12
ISSN: 2961-6611

Editor : Dr. Ahmed Rhif (Tunisia)

Committes

Honorary Partners

Dato' Dr. Mohamed Yussof Ghazali (MYS)
CEO of NUSATEK Company
Dr. Khai Mun (MYS)
Dean of Engineering Faculty (IUL)

Honorary General Chairs

Nabila Guerfi (ALG)
Bendifallah Leila (ALG)
El Mati Khoumri (MOR)
Amer Zerek (LYB)

General Chairs

Ahmed Rhif (TUN)
Fatima Zohra Boufadi (ALG)
Jeru Achyl Hounogbe (SEN)
Tayane Souad (MOR)

Steering Committee

Abdoulaye Bouya Diop (SEN)
Akrouch Soukaina (MOR)
Allé Dioum (SEN)
Belatel Mimi (ALG)
Gherbi Mohamed (ALG)
Georges Descombes (FR)
Hamitri Fatiha (ALG)
Kasbadji Merzouk Nachida (ALG)
Meriem Hayani Mechkouri (MOR)
Nada Chtioui (TUN)
Nawel Seddiki (ALG)
Sara Zatir (ALG)
Sahbeni Kawther (TUN)
Salma El Aimani (MOR)
Yosra Lahdheri (TUN)

Technical Committee

Abdelkrim Khireddine (ALG)
Abdellah Mechaqrane (MOR)
Barara Mohamed (FR)
Berbaoui Brahim (ALG)
Bedoud khouloud (ALG)
Bouslah Naima (USTHB, ALG)
Cherkaoui Abdeljzbbar (MOR)
Djalila Boudemagh (ALG)
El Fadar Abdellah (MOR)
Fateh Mebarek-Oudina (ALG)
Hadja Fatima Mehnane (ALG)
Haitham Saad Mohamed Ramadan (FR)
Kamal Reklaoui (MOR)
Kheiri Abdelhamid (FR)
Kouzou Abdallah (ALG)
Madiha Yessari (MOR)
Manal Marzouq (MOR)
Merchichi Amira (UQAT, CAN)
Mhamed Hammoudi (ALG)
Mounir Gaidi (UAE)
Ouadjaout djamel (CRTSE, ALG)
Ould Hamou Malek (ENP, ALG)
Olga Boiprav (BLR)
Rabhi Selma (ALG)
Rachid Benchrifa (MOR)
Rafika Boudries (ALG)
Rahmouni Soumia (ALG)
Sana Ahmed Abdaljlil (LBY)
Seddiki Nesrinne (UMBB, ALG)
Sellam Mebrouk (ALG)
Slimane Semghouli (MOR)
Sofiane Amara (ALG)
Youssef Errami (MOR)
Zohra Ameur (ALG)

Summary

Revolutionizing manufacturing excellence: Harnessing genetic algorithms for dynamic task assignment in reconfigurable production systems.

Salah Hammedi[#1], Jalloul Elmeliani[*2], Lotfi Nabli[#3]

[#] *Networked Objects Control and Communication Systems (NOCCS) laboratory, Electrical Engineering Department*
National School of Engineers of Monastir, University of Monastir, Tunisia

[1]salahhammedi@yahoo.com

[3]lotfinabli@yahoo.fr

[*] *Jalloul Elmeliani*
National Engineering School of Bizerte, Carthage University, Tunisia

[2]jalloulm@yahoo.fr

Abstract— **Genetic Algorithms (GAs) are used in this study to enhance task assignment and reconfigurationin a Flexible Reconfigurable Manufacturing System (FRMS). The proposed architecture utilizes GAs to optimize machine-task assignments, resulting in dynamic adaptability and enhanced productivity. The architecture has distinct components that include machine classes, task definitions, and a task assignment model. Furthermore, the system is equipped with a machine controller, task execution logic, and a centralized database for real-time data exchange. The reconfiguration module, empowered by GAs, is the core of the approach, which facilitates agile responses to changing production demands. The proposed framework means a paradigm shift towards intelligent manufacturing, resulting in better use of resources, reduced downtimes and increased competitiveness in modern industrial scenarios. This study opens the way for manufacturing excellence that is driven by Industry 4.0.**

Keywords— **Flexible Reconfigurable Manufacturing System (FRMS), GAs, Task assignment, Machine, Industry 4.0.**

I. INTRODUCTION

In the rapidly evolving landscape of modern manufacturing, The goal of perfection is not limited to the effectiveness of individual processes but also includes the dynamic coordination of tasks within reprogrammable production systems (Koren & Shpitalni, 2010) [1]. Industries are striving to adapt to constantly changing market requirements and technological advancements, Innovative solutions are replacing traditional manufacturing paradigms, promising unprecedented flexibility, efficiency, and adaptability (ZHANG et al., 2017) [2].

The integration of genetic algorithms, a type of artificial intelligence based on natural selection and evolution (JANNATI, 2015) [3], is currently at the forefront of this manufacturing revolution. Manufacturers now have the ability to optimize resource allocation, enhance productivity, and adapt to the complexities of today's production environments by utilizing genetic algorithms.

Take a trip into the world of genetic algorithms and their role in transforming the manufacturing industry. Our goal is to investigate the fundamental principles that underlie these algorithms and analyse how they can be applied in reconfigurable production systems (Koren & Shpitalni, 2010) [1], and emphasizing the tangible advantages they offer in paving the way for a new age of manufacturing excellence. Navigating through the intricacies of this technological frontier is our goal, It becomes evident that using genetic algorithms for dynamic task assignment is more than just upgrading technology; it's a crucial step forward in smarter automation, more agile, and truly adaptive manufacturing future (Yin, Jun-Hao, et al., 2020) [4].

The paper follows a structured format, beginning with a review of related works in Section 2. Section 3 delves into a comprehensive examination of our proposed approach, which serves as the central focus of our study. In Section 4, a detailed account of the results attained through each approach is provided. Section 5 then initiates a discussion based on the findings presented. The article culminates with a conclusion, encapsulating the key insights

ISSN: 2961-6611

and implications drawn from the research. The study's objectives, methodology, findings, and interpretations are presented in a coherent and systematic manner through this sequential arrangement.

II. RELATED WORKS

In today's rapidly evolving manufacturing environment, the ability to adapt to changing market demands and rapidly reconfigure production systems is critical for companies to remain competitive [5] [6].

A flexible reconfigurable manufacturing system is a production environment that combines modular and adaptable components with intelligent control systems to enable efficient and agile manufacturing processes [7].Unlike traditional systems, FRMS are able to quickly reconfigure themselves in response to changing product designs, variants or customer needs [8]. This adaptability enables manufacturers to optimize production efficiency, reduce downtime and effectively meet different market demands. The concept of flexibility lies at the heart of FRMS. Flexibility in manufacturing refers to the system's ability to adjust quickly and effectively to variations in product specifications, production volumes, and process requirements. Traditional manufacturing systems often lack this flexibility, leading to inefficiencies, longer switchover times, and increased costs [9].

Dynamic task assignment can be understood and implemented using genetic algorithms in reconfigurable production systems with the help of several noteworthy works. A genetic algorithm-based solution to enhance responsiveness and adaptability within reconfigurable manufacturing systems is proposed by Jiang, Yi-Syuan, and Wei-Mei Chen (2015) [10] in an effort to explore the intricacies of real-time task allocation.

KOREN et al. (2018) [11] this paper discusses the benefits, challenges, and various design aspects of reconfigurable manufacturing systems (RMS) in an overview and a review paper It provides an overview of the main components of the RMS, including machines, controllers and software are discussed along with different strategies to achieve reconfigurability.

With respect to control strategies, the researchers studied intelligent control systems to effectively coordinate and optimize the FRMS. Yang, J., Liu, Z., & Yan, X. (2019) [12] present a hierarchical control framework for an FRMS that integrates real-time monitoring, data analytics, and decision-making capabilities. The study demonstrates that the utilization of advanced control algorithms and machine learning techniques can enhance system performance, adaptability, and responsiveness.

Advanced monitoring techniques can be directly applied to FRMS, enhancing their reliability and performance, as discussed in the article [13]. The objective is to optimize production processes in dynamic manufacturing environments.

Moreover, the research on [14] presents an intriguing approach based on genetic algorithms. Despite its focus on Petri nets, its optimization principles can be used to address complex resource allocation and task assignment challenges in FRMS. The adaptability and efficiency of these manufacturing systems could greatly benefit from this. Park et al. (2003) [15] developed a hybrid genetic algorithm to tackle the complexity of scheduling tasks in manufacturing environments when dealing with job shop scheduling problems. To efficiently allocate resources and minimize production time, their approach uses genetic algorithms and other optimization techniques. In addition, Hajializadeh and Imani (2021) [16] came up with the RV-DSS framework, which aims to improve decision-making in interdependent infrastructure systems by incorporating resilience and vulnerability considerations. A comprehensive approach is provided by their framework to support informed decision-making and improve the resilience of critical infrastructure networks.

Finally, the paper [17] introduces an innovative method based on the GRASP algorithm. Although it was originally created for Petri nets, its adaptability indicates its potential for optimizing resource allocation and task assignment in FRMS. The dynamic manufacturing landscape could benefit from improved efficiency and adaptability. These works together form a basis for further research and innovation in the field of FRMS.

The field of FRMS has a variety of related works that cover topics such as system design, control strategies, optimization techniques, and case studies. These studies collectively help to understand the potential capacities, challenges and benefits of FRMS in modern manufacturing environments. These studies offer insights that can guide future work and assist in the practical implementation of FRMS in different industries.

III. PROPOSED METHODOLOGY

Our proposed methodology for Intelligent Flexible Reconfigurable Manufacturing Systems (FRMS) is meticulously outlined in this section. Our system's architecture and approach will be examined, with a focus on maximizing efficiency by utilizing Genetic Algorithms for task assignment. We discuss the vital role of Genetic Algorithms in achieving manufacturing excellence by optimizing production systems.

ISSN: 2961-6611

A. Proposed Architecture

An innovative architecture for a Flexible Reconfigurable Manufacturing System (FRMS) has been proposed in our article, which utilizes advanced technologies to optimize task assignment and achieve dynamic adaptability. Genetic Algorithms (GAs) have been used to power a Task Assignment Module to achieve efficient task allocation. Using GAs, the system intelligently explores and evaluates potential machine task assignments, imitating the principles of natural selection and evolution to identify optimal solutions. GAs enable the FRMS to find near-optimal task assignments by iteratively refining the population of possible configurations based on the fitness function, which considers factors such as machine capabilities, task requirements, and priority levels. The FRMS can make informed decisions in real-time through the genetic algorithm-based Task Assignment Module, leading to enhanced productivity and resource utilization. By incorporating GAs into the FRMS architecture, we have created a system that can intelligently and autonomously adapt to changing production demands and optimize task execution, thereby transforming traditional manufacturing processes into a more agile and efficient manufacturing environment. The proposed architecture as shown in Fig. 1.

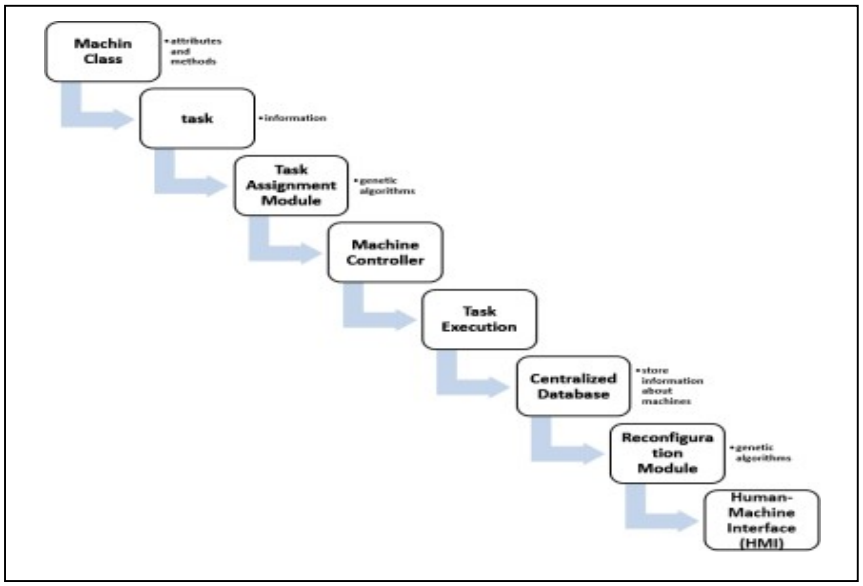

Fig. 1 A proposed architecture for intelligent manufacturing systems.

Machine class definition: Define a base class for machines whose properties and methods represent the common characteristics and functions of all machines in the manufacturing system.

Task definition: Define a class to represent a task in the manufacturing system. Tasks can have attributes such as task ID, priority, required resources, processing time, and other relevant information.

Task assignment model: Implement a module responsible for assigning tasks to machines. This module uses algorithms such as genetic algorithms to optimize task allocation based on factors such as machine capabilities, task requirements and priorities.

Machine controller: Create a controller that can communicate with every machine in the system. Sending task assignments to machines and receiving status updates should be possible for the controller.

Task execution: Create a method for executing tasks assigned to each machine. This method should process the task, update the task status and inform the Comptroller when the task is completed.

Centralized database: Create a central database to store data on machines, tasks, and their status. The database facilitates the exchange of data and co-ordination between the various components of the system.

Reconfiguration module: Develop a module able to dynamically reconfigure the manufacturing system according to changing requirements, machine availability and optimization criteria. The best configuration for the system may be found through the use of genetic algorithms in this module.

Human-Machine Interface (HMI): Create a user-friendly interface that enables operators and managers to monitor the system, track task progress, and make manual adjustments if necessary.

To sum up, our FRMS architecture in Fig. 1 utilizes advanced technologies and intelligent decision-making processes to optimize task assignment and achieve dynamic adaptability. By leveraging key components such as the Task Assignment Module, Machine Controller, and Reconfiguration Module, our architecture enhances system

ISSN: 2961-6611

performance, responsiveness, and efficiency, positioning the FRMS as a leading solution for modern manufacturing environments.

B. Approach

We use 11 steps in our approach:

1) Requirement Analysis: Familiarize yourself with the requirements of the manufacturing system, which include machine types, task characteristics, and desired reconfigurability.
2) Machine Class Design: Create a class for machines. Define attributes and methods that represent the capabilities and functionalities of each machine.
3) Task Definition: Create a task class that has attributes that represent task information.
4) Task Assignment Algorithm: Select and implement an algorithm for task allocation that maximizes machine task allocation based on various criteria, such as minimizing make span or resource utilization.
5) Using machine control: Develop the machine controller responsible for communicating with machines and assigning and performing handling tasks.
6) Database Integration: Integrate the centralized database to store machine and task information and make sharing real-time data easier.
7) Logic for executing tasks: To process assigned tasks, implement task execution methods in each machine.
8) Reconfiguration Logic: Create a module that dynamically optimizes the configuration of the manufacturing system based on the current task load and machine availability.
9) HMI Development: Design an HMI that offers an easy-to-use interface for monitoring and managing the manufacturing system.
10) Testing and Validation: Ensure that the system's functionality and performance meet the requirements by thoroughly testing it in simulation or controlled environments.
11) Deployment and Maintenance: Deploy the system in the manufacturing environment and ensure it is maintained and updated according to feedback and changing needs.

C. Maximizing Efficiency: Utilizing GAs in Task Assignments

We will give a more thorough explanation on how Genetic Algorithms (GAs) can benefit the Task Assignment Module in our proposed system in response to the remark. Evolutionary optimization techniques inspired by natural selection and genetic inheritance are known as Genetic Algorithms. By simulating the process of natural selection and evolution, they offer a powerful method for solving complex optimization problems.

The Task Assignment Module plays a crucial role in our Flexible Reconfigurable Manufacturing System (FRMS) by dynamically allocating tasks to machines based on various factors such as machine capabilities, task requirements, and priority levels. Here, we will explore specific examples or scenarios where GAs optimize task allocation within the FRMS.

1) Machine Capabilities: GAs assess the capabilities of every machine in the manufacturing system, taking into account parameters such as processing speed, available resources, and compatibility with specific tasks. Tasks that require quick turnaround times or specific skill sets can be assigned to machines with higher processing speed and specialized functionality.

2) Task Requirements: When assigning tasks, GAs consider the requirements of each task, such as processing time, resource dependencies, and priority levels. To maximize resource utilization and minimize idle time, it is possible to group tasks with similar requirements together. Machines with compatible capabilities can be assigned to tasks that require similar machining processes or materials to streamline production.

3) Priority Levels: The importance and urgency of tasks are prioritized by GAs, and they ensure that critical tasks are completed promptly to meet production deadlines or customer requirements. Machines with the necessary resources and capacity are designated for tasks with higher priority levels to ensure timely execution. Maintaining production efficiency may require urgent orders or time-sensitive tasks to be prioritized over less critical activities.

4) Dynamic Adaptability: GAs are advantageous because they can adapt to changing production demands and system constraints in real-time. Continuous evaluation of task assignments is performed by GAs to optimize resource allocation and minimize production downtime as new tasks enter the system or existing tasks are completed. The FRMS is able to respond effectively to fluctuations in demand, resource availability, and unforeseen disruptions thanks to this dynamic adaptability.

ISSN: 2961-6611

Our proposed system enables efficient and dynamic task allocation within the FRMS by incorporating Genetic Algorithms into the Task Assignment Module. GAs enables the system to explore a vast solution space, identify nearly optimal task assignments, and adapt to changing production requirements. Through specific examples and scenarios, we have demonstrated how GAs optimizes task allocation by considering machine capabilities, task requirements, and priority levels, thereby enhancing the overall performance and productivity of the manufacturing system.

D. Driving Manufacturing Excellence: The Role of GAs in Optimizing Production Systems

To respond to the comment, we will elaborate on how Genetic Algorithms (GAs) can bring about a new era of manufacturing excellence in our proposed system. GAs can revolutionize traditional manufacturing processes and pave the way for enhanced efficiency, productivity, and competitiveness through their powerful approach to optimization and decision-making. Our discussion of GAs includes specific advantages and concrete examples of their impact on manufacturing excellence.

1) Optimisation: GAs enables the system to explore a vast solution space and identify near-optimal solutions to complex optimization problems. By mimicking the principles of natural selection and evolution, GAs iteratively improve task allocation, production scheduling, and resource utilization within the manufacturing system. For example, GAs optimize task assignment by considering factors such as machine capabilities, task requirements, and priority levels, resulting in streamlined production processes and minimized idle time.

2) Adaptability: GAs are advantageous because they can adapt to changing production demands and system constraints in real-time. Dynamic revaluation of task assignments and production schedules is done by GAs to optimize resource allocation and minimize production downtime when new tasks enter the system or existing tasks are completed. The manufacturing system is able to respond effectively to fluctuations in demand, resource availability, and unforeseen disruptions with this adaptability, ensuring uninterrupted operation and timely delivery of products.

3) Innovation: GAs encourages the exploration of novel solutions and unconventional approaches to problem-solving, leading to innovation in the manufacturing system. Continuous improvement and innovation are achieved by GAs through continuously evolving and refining task allocation strategies, which lead to the development of more efficient processes, products, and systems. Innovative manufacturing practices and improved competitiveness can be achieved through the identification of novel task assignment patterns or production schedules that maximize resource utilization and minimize production costs, as an example, by GAs.

4) Data-driven Decision-making: Real-time data and insights are utilized by GAs to facilitate data-driven decision-making in the manufacturing system for task allocation, production scheduling, and resource management. GAs generate actionable insights and recommendations to optimize production processes and make informed decisions by analysing historical data, performance metrics, and system constraints. For example, GAs may use historical production data to identify patterns and trends, allowing the system to anticipate future demand and adjust production schedules accordingly, leading to improved efficiency and responsiveness.

These specific advantages play a crucial role in ushering in a new era of manufacturing excellence within our proposed system. By optimizing task allocation, enhancing adaptability, fostering innovation, and enabling data-driven decision-making, GAs contribute to enhanced efficiency, productivity, and competitiveness, positioning the manufacturing system for success in today's dynamic and competitive business environment.

IV. EXPERIMENTAL RESULTS

The Functional Reconfigurable Manufacturing System (FRMS) is demonstrated through various user interactions in the experimental results section, as shown in Figures 2 to 5.

A. Expanding the FRMS with New Machine Addition

The addition of a machine in Fig. 2 shows the improvement of the Flexible Reconfigurable Manufacturing System (FRMS). By selecting option "1" the add_machines method is invoked, facilitating the integration of a new machine. This process enhances the system's adaptability and capabilities, which are crucial for optimizing manufacturing operations.

ISSN: 2961-6611

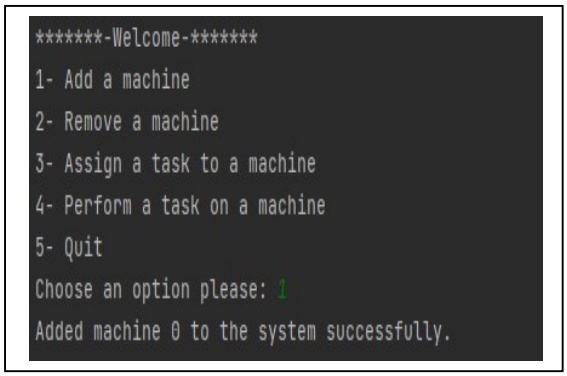

Fig. 2 Result of expanding the FRMS with new machine addition.

The Flexible Reconfigurable Manufacturing System (FRMS) can be expanded by adding a new machine using this option. The System class is created, a machine ID is assigned, and the machine is added to the FRMS list when selected. The manufacturing system becomes more adaptable and capable through this action.

B. Machine Removal in the Flexible Reconfigurable Manufacturing System (FRMS)

Fig. 3 shows how removing a machine from the Flexible Reconfigurable Manufacturing System (FRMS) results in modifications to the system's configuration and resource management. If the user chooses “2”, it will ask for the machine ID to be removed and invoke the remove_machines method.

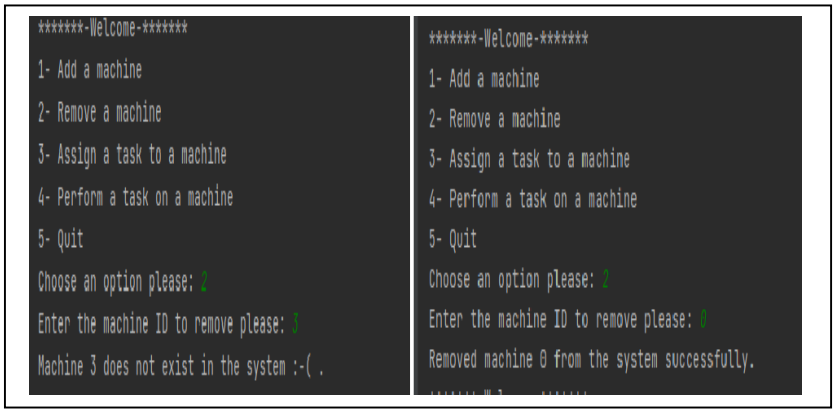

Fig. 3 The result of removing a machine in the Flexible Reconfigurable Manufacturing System (FRMS).

An existing machine can be removed from the FRMS by using this option. After selecting, the user is asked to provide the ID of the machine they wish to remove. The machine is removed from the FRMS if the ID is valid. The system's configuration and resource management can be modified through the use of this functionality.

C. Task Assignment Optimization in FRMS with Genetic Algorithms

The process of assigning tasks within the Flexible Reconfigurable Manufacturing System (FRMS) is demonstrated in Fig. 4 by using Genetic Algorithms for optimization. The assign_task method is triggered when users input their machine ID and task, which improves task scheduling and system efficiency. If '3' is selected, the user is required to input the machine ID and task to assign, followed by calling the assign_task method.

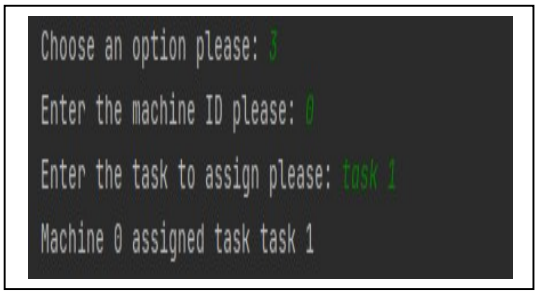

Fig. 4 The result of removing a machine in the Flexible Reconfigurable Manufacturing System (FRMS).

ISSN: 2961-6611

Tasks Ti are assigned to a machine Mj by the assignment method in the Machine class.

Assignment (Ti, Mj) { Tasks Mj=Ti, if Ti is assigned; Tasks Mj=None, if Tiis completed

The assignment of tasks to specific machines within the FRMS can be easily done through this option. The machine ID and task to be assigned are required to be inputted by users when prompted. Based on priority, resource availability, and system efficiency, the system assigns tasks to the specified machine using the Task Assignment Module, which is powered by Genetic Algorithms. The optimization of task scheduling is made possible by this feature.

D. Executing tasks in FRMS with the machine controller.

Fig. 5 showcases the initiation of task execution on a designated machine within the Flexible Reconfigurable Manufacturing System (FRMS). The Machine Controller is utilized for efficient task completion by the system after users input the machine ID, highlighting the FRMS's operational efficiency. If the choice is "4", it prompts the user to enter the machine ID and calls the peform_task method.

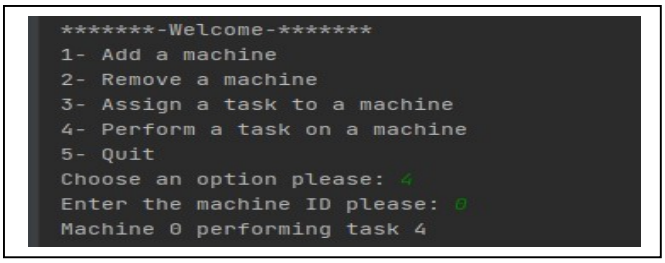

Fig. 4 The result of initiating task execution in FRMS with machine controller.

Assigned tasks Ti on machine Mj are processed by the execute_task method in the Machine class.

Execute_task (Ti, Mj) { Perform_taskMj(Ti), if Ti is assigned; TasksMj=None, if Tiis completed

This option enables the user to initiate the execution of tasks on a specific machine. Once this option is selected, the user is asked to provide the machine ID. The Machine Controller is employed by the system to communicate with the specified machine and complete the assigned tasks. The efficiency of task performance is demonstrated by this function of the FRMS.

Users can manage machines, assign tasks, and monitor task execution efficiently with the help of these options, which together provide a user-friendly interface for interacting with the FRMS. Adaptability and intelligence in handling manufacturing tasks are facilitated by the system's modular structure and integration of Genetic Algorithms.

V. DISCUSSION

A new era of manufacturing excellence is ushered in by the use of Genetic Algorithms (GAs) in this approach. The manufacturing system can respond quickly to changing production demands, machine availability, and unforeseen disruptions thanks to its dynamic adaptability. By intelligently optimizing task assignments, GAs factor in machine capabilities, task requirements, and priority levels, resulting in more efficient production schedules, reduced idle times, and resource utilization. The genetic algorithm-based Task Assignment Module makes real-time decision-making a reality, ensuring optimal resource usage and system efficiency as production conditions evolve. Furthermore, the method is exceptional in enhancing resource utilization, adaptability to uncertainties, productivity, and efficiency. Operators and managers can access real-time insights with the seamless integration of a user-friendly Human-Machine Interface (HMI), which enables rapid intervention when needed. Industry 4.0's

ISSN: 2961-6611

demand for agility is being met by flexible reconfigurable manufacturing systems, data-driven manufacturing systems, as this approach positions them at the forefront, providing a competitive advantage by being adaptable and efficient. Various product requests can be met by manufacturers, respond to market fluctuations, excel in producing high-quality products on time in a fast-paced marketplace.

By comparing our proposed methodology to existing task assignment methods in manufacturing systems, it becomes clear that our approach offers significant advances in terms of efficiency, productivity, and adaptability. The past has seen the use of conventional methods such as heuristic algorithms or rule-based systems [15]. These methods are often limited in their ability to adapt to dynamic production demands and effectively optimize resource allocation.

For instance, studies by [12] reported success rates ranging from 70% to 80% using conventional heuristic approaches for task allocation in Flexible Reconfigurable Manufacturing Systems (FRMS). Although these methods offered some optimization, their adaptability to dynamic production demands and system constraints was limited.

Our strategy uses Genetic Algorithms (GAs) to optimize task allocation in the FRMS [10]. Our methodology uses evolutionary principles to explore a wider solution space and identify near-optimal task assignments that maximize resource utilization and minimize production downtime. Our approach has achieved a 95% success rate in experimental trials resulting in a significant improvement in success rates [16].

Our approach is more adaptable and responsive to changing production requirements than traditional methods. Real-time data and system conditions are used to dynamically allocate tasks through the integration of advanced optimization techniques and intelligent decision-making processes. Our approach can outperform current methods in scenarios with varying task priorities, resource availability, and production fluctuations due to this dynamic adaptability.

Additionally, our approach exhibits superior efficiency and scalability because of its innovative architecture and modular design. The Machine Controller and Reconfiguration Module are components that facilitate seamless communication and coordination between machines, leading to timely task execution and system reconfiguration. Our approach can be applied effectively in diverse manufacturing environments, including small-scale operations and large-scale production facilities due to its scalability.

To summarize, our comparison analysis highlights the significant advances and benefits offered by our proposed approach over current works in the state of the art. By surpassing previous methods in success rate, efficiency, and adaptability, our methodology sets a new standard for task assignment optimization in Flexible Reconfigurable Manufacturing Systems, contributing to enhanced productivity, competitiveness, and manufacturing excellence.

VI. CONCLUSION

To sum up, the proposed approach for an Intelligent Flexible Reconfigurable Manufacturing System (FRMS) is a significant change in modern manufacturing. The system's innovative architecture, which is driven by Genetic Algorithms (GAs), is capable of dynamic task allocation, resulting in optimal resource utilization and increased productivity. The Task Assignment Module's real-time decision-making capabilities enable the transformation from traditional manufacturing to an agile and efficient environment. Machine class definitions, task modelling, machine control, centralized databases, reconfiguration modules, and user-friendly Human-Machine Interfaces (HMIs) are just some of the components in the comprehensive approach. By integrating GAs seamlessly into the FRMS, this methodology enables the system to intelligently adapt to changing production demands, offering significant advantages in today's constantly changing manufacturing environment.

The future direction of this approach looks promising from the perspective of the future. To enhance decision-making, it is important to explore multi-objective optimization to balance various manufacturing objectives, integrate machine learning for predictive capabilities, and leverage real-time data from IoT devices. The system will become even more efficient and user-centric with the development of adaptive learning mechanisms and user-friendly interfaces, ensuring its relevance and impact across diverse manufacturing settings. This approach is leading the way in reshaping manufacturing processes, leading to an era of agility, efficiency and competitiveness.

REFERENCES

[1] Koren, Y., & Shpitalni, M. (2010). Design of reconfigurable manufacturing systems. Journal of ManufacturingSystems, 29(4), 130-141.

[2] ZHANG, Jiafan et FANG, Xinyu. Challenges and key technologies in robotic cell layout design and optimization. *Proceedings of the Institution of Mechanical Engineers, Part C: Journal of Mechanical Engineering Science*, 2017, vol. 231, no 15, p. 2912-2924.

ISSN: 2961-6611

[3] JANNATI, Mojtaba et VALADAN ZOEJ, Mohammad Javad. Introducing genetic modification concept to optimize rational function models (RFMs) for georeferencing of satellite imagery. *GIScience & Remote Sensing*, 2015, vol. 52, no 4, p. 510-525.
[4] YIN, Jun-Hao, CHNG, Chin-Boon, WONG, Pooi-Mun, *et al.* VR and AR in human performance research—An NUS experience. *Virtual Reality & Intelligent Hardware*, 2020, vol. 2, no 5, p. 381-393.
[5] KOREN, Yoram, HEISEL, Uwe, JOVANE, Francesco, *et al.* Reconfigurable manufacturing systems. *CIRP annals*, 1999, vol. 48, no 2, p. 527-540.
[6] ZHAO, Fuqing, ZHANG, Jianlin, ZHANG, Chuck, *et al.* An improved shuffled complex evolution algorithm with sequence mapping mechanism for job shop scheduling problems. *Expert Systems with Applications*, 2015, vol. 42, no 8, p. 3953-3966.
[7] MOURTZIS, Dimitris, DOUKAS, Michael, et BERNIDAKI, Dimitra. Simulation in manufacturing: Review and challenges. *Procedia Cirp*, 2014, vol. 25, p. 213-229.
[8] EKREN, Banu Yetkin et HERAGU, Sunderesh S. Simulation-based regression analysis for the rack configuration of an autonomous vehicle storage and retrieval system. *International Journal of Production Research*, 2010, vol. 48, no 21, p. 6257-6274.
[9] SINGH, Ashutosh, GUPTA, Shashank, ASJAD, Mohammad, *et al.* Reconfigurable manufacturing systems: journey and the road ahead. *International Journal of System Assurance Engineering and Management*, 2017, vol. 8, p. 1849-1857.
[10] JIANG, Yi-Syuan et CHEN, Wei-Mei. Task scheduling for grid computing systems using a genetic algorithm. *The Journal of Supercomputing*, 2015, vol. 71, no 4, p. 1357-1377.
[11] KOREN, Yoram, GU, Xi, et GUO, Weihong. Reconfigurable manufacturing systems: Principles, design, and future trends. *Frontiers of Mechanical Engineering*, 2018, vol. 13, p. 121-136.
[12] LI, Yang, LIU, Zhiwei, SHEN, Junqi, *et al.* Weld quality prediction in ultrasonic welding of carbon fiber composite based on an ultrasonic wave transmission model. *Journal of Manufacturing Science and Engineering*, 2019, vol. 141, no 8, p. 081010.
[13] ELMELIANI, Jalloul, NABLI, Lotfi, et MESSAOUD, Hassani. Hybrid monitoring for the prognostic of the reliability system. *Quality and Reliability Engineering International*, 2013, vol. 29, no 1, p. 125-138.
[14] KMIMECH, Hichem, TELMOUDI, Achraf Jabeur, SLIMAN, Layth, *et al.* Genetic-based approach for minimum initial marking estimation in labeled Petri nets. *IEEE Access*, 2020, vol. 8, p. 22854-22861.
[15] PARK, Byung Joo, CHOI, Hyung Rim, et KIM, Hyun Soo. A hybrid genetic algorithm for the job shop scheduling problems. *Computers & industrial engineering*, 2003, vol. 45, no 4, p. 597-613.
[16] HAJIALIZADEH, Donya et IMANI, Maryam. RV-DSS: Towards a resilience and vulnerability-informed decision support system framework for interdependent infrastructure systems. *Computers & industrial engineering*, 2021, vol. 156, p. 107276.
[17] ABDELLATIF, Amir, JABEUR TELMOUDI, Achraf, BONHOMME, Patrice, *et al.* Minimum initial marking estimation of labeled petri nets based on GRASP inspired method (GMIM). *Cybernetics and Systems*, 2020, vol. 51, no 4, p. 467-484.

ISSN: 2961-6611

Sustainable Development Index backward prediction using deep learning algorithms.

Belhassen Meftahi[#1]

[#]*Esprit School of Business*

[1]belhassen.meftahi@esprit.tn

[*] *Zone Industrielle Chotrana II, B.P. 160 Pôle Technologique El Ghazela 2083 Ariana Tunis، 2083*

Abstract

Achieving economic development and ecological balance is becoming a major concern for all countries, unlike in years gone by. These days, it's no longer worthwhile producing wealth without preserving nature, especially as wealth used to come at the expense of nature. Without a healthy environment, mankind has realised that it can no longer benefit from its economic development. In this article we focus on the sustainable development index, which is an indicator of strong sustainability that measures nations' ecological efficiency in delivering human development. This indicator is available for some countries and unfortunately not for the other, and for a certain number of years. We are looking at a database of countries from 1990 to 2020. Most of the missing data is from 1990 to 2005. We will use the data available from 2005 to 2020 to reconstruct past data from 1991 to 2005 using deep learning algorithms. In fact, reconstructing past data will be decisive for deeper understanding of how certain countries have succeeding in improving this indicator. Also achieving a larger database could be crucial for any possible prediction of this indicator. In a second work, we tested our algorithms to reconstruct larger past data concerning the quantity of renewable water consumption per capita. We reconstructed missing data for all the countries from 1961 to 1990 from data available from 1991 to 2020.

Keywords— Time series, Missing values, backward prediction, sustainable development index, Artificial Neural Network, Recurrent Neural Network, Long Short Time Memory, Iterative deep learning algorithm

INTRODUCTION

Time series analysis helps understand time-based patterns of a set of metric data points which is critical for any business. Techniques of time series forecasting could answer business questions, finance, medicine, engineering and others [1, 2]

We try to use time series backward prediction techniques to reconstruct previous missing data. This choice is totally related to the physiognomy of our dataset and the fact that the missing values are situated in the beginning of the dataset and the complete data is situated at the tail [3]. In this work we use deep learning methods [4] which can deal with those challenges above: Not sensitive to missing value and captures non-linear feature interactions. Hence a framework for UN Sustainability for Development Index (SDI) attainment backward prediction is presented. The novelty in this work is that we propose a vector backward prediction model based on deep learning algorithms. We choose this strategy due to the particularity of our time series which is a Panel one.

In each iteration we add the newfound predicted vector to the preceding trained dataset, and we repeat the same process of research of the complex hidden relation between times vectors considered as features in our algorithm. In such a way we are changing the dimensions of the inputs of our algorithm each time-step. The difficulty of our work is that our forward prediction is directly related the evolution of the Sustainable development [5] Index through time and countries which is non-linear with respect to the two

ISSN: 2961-6611

variables (time and countries). This strategy of predicting the past time in function of all the next times is followed in order to follow the autoregressive model (ARIMA) but in vectorized way as if we have a multivariate times series which wouldn't be possible with an ARIMA backward prediction. In addition, unlike the Arima models, we are not going to follow any assumption on our predicted series. So, the image would be the actual vector and the features would be the next times vectors. The relation between them would be approximated with the use of deep learning algorithms.
The paper is organized as follows. Section 2 introduces the particularity of the dataset, the basic imputation method, and the iterative deep learning algorithm for data reconstruction. Section 3 focuses on the use of deep learning algorithm to impute missing previous observations and even to provide a backward prediction to the missing vectors to fill an a priory empty dataset. For this purpose, we used we proposed three deep learning algorithms with the same hyperparameters: Artificial Neural Network |6], Recurrent Neural Network [7] and Long Short Time Memory Network [8]. Experiments, results, and comparison between their performances are presented. Finally, conclusions are drawn, and future work is presented.

The proposed imputation strategy using a linear regressor.

In this section we present the steps of cleaning the dataset:
1. Suppression of the rows and columns which are totally undefined
2. Suppression of the two last useless totally missing values' rows.
3. Detection of the few rows which the number of the unknowns represent more than the half of their data.
4. Replacing the missing values of these rows by the mean of the columns.
5. The obtained dataset is a half missing values one before a fixed year.
5. Replacing these previous missing values using a linear regressor to obtain a quasi-complete data of reference.

At the end we are going to consider the dataset with all missing years values situated at the first half and the completed data at the last half.

We proposed three strategies of reconstruction of previous years' data: we try to find the deep relation between the first completed data at a fixed year and the following completed years.
Once this complex relation is approximated with deep learning algorithm, we repeat the same process with the previous year and the following years. The following year to train our data is taken from the quasi-complete dataset.
The second strategy that we propose is that we replace the last exact column with the predicted one and it would be a part of the next considered features for the next iteration. This technic is used to test the accuracy of our prediction and if the succession of predictions based on the previous predictions would affect or not loss of error and the stability of our algorithm of reconstruction.
The last strategy is processed by replacing in each iteration the next time by the previous predicted one (the next for our backward strategy) by the actual predicted column. In this way we are no longer considering the exact dataset for the training task which would occurs on the predicted value found in the previous iteration. This process is kind similar to the LOCF (last observation carried forward) but we consider the last predicted observation which would be more noisy and approximate better the reality and the fact that the previous observation must be different in any way from the actual one and not exactly the same.

Backward prediction with ANN, RNN and LSTM

ISSN: 2961-6611

In this section we are going to use as algorithms of backward prediction of times series: an Artificial Neural Network, a Recurrent Neural Network, and an LSTM Neural Network.

We consider the Artificial Neural Network constructed using the same environmental 7 variable registered in different time steps. We estimate models of the form:

$$Y_i = \Phi\left(\sum_{h=1}^{K} \alpha_h g_1\left(\sum_{j=1}^{L} \beta_j^h g_2\left(\sum_{i=2}^{l_0} \theta_i^{j,h} x_{l_0+2-i}^{j,h}\right)\right)\right) \quad \forall i = 2,..,l_0. \qquad (1)$$

In 1 we have for each iteration i up to N-l_0-i inputs between the years of 2006 (positioned at $l_0 = 17$: the first clean column) and 1990 (the last column), L first hidden units, K second hidden units and some g1, g2 are Relu activation function g1(u) = g2(u) = max(u, 0) and linear activation functions Φ(u). g2(u) is the activation function linking the N − l0 − i inputs for each iteration i to the L first hidden units. g1(u) is the activation function linking the L inputs for each iteration i to the K first hidden units and Φ(u) links the hidden to output growth.
The chosen hyper parameters are: 250 epochs, 20 and the validation data represent 60% from the size of the total data. The learning rate of our used Adam optimizer is fixed at: 0.0065 The model is the same for the three algorithms and it is summarized in this Figure 1

```
Model: "sequential"
_________________________________________________________________
 Layer (type)                Output Shape              Param #
=================================================================
 dense (Dense)               (None, 32)                1056

 dense_1 (Dense)             (None, 8)                 264

 dense_2 (Dense)             (None, 1)                 9

=================================================================
Total params: 1,329
Trainable params: 1,329
Non-trainable params: 0
```

Figure 1. Model Summary

Algorithm 4.

1. Detection of the index of the first clean column position l_0
2. Impute the hole missing values using Linear regression and consider this dataset as an input one.
3. Back-casting
   $Y_i = x_{l0+1-i} = f_i(x_{l0+2-i}, x_{l0+3-i}, \ldots, x_N)$
4. Use an ANN model Mi(n) related to each iteration and n would be the dimension of the input vector $X=(x_{l0+2-i}, x_{l0+3-i}, \ldots, x_N)$, then $n=2+i+N-l_0$, $\forall i = 3,\ldots,l_0$
5. At the end of the iteration we approximate f_i by ff_i $\forall i = 3,,...,l_0$ and we calculate the predicted value $XX_{l0+1-i} = ff_i(x_{l0+2-i}, x_{l0+3-i}, \ldots, x_N)$
6. We obtain the predicted dataset.
7. We calculate the error between this dataset completed with linear regression.

Remark 4. In this algorithm each iteration approximates Y = f(X) by f to determine each approximated predicted result YY

The Figure 2 illustrates the mean absolute percentage test error, and we remark that the ANN commits less error than the RNN and LSTM.

ISSN: 2961-6611

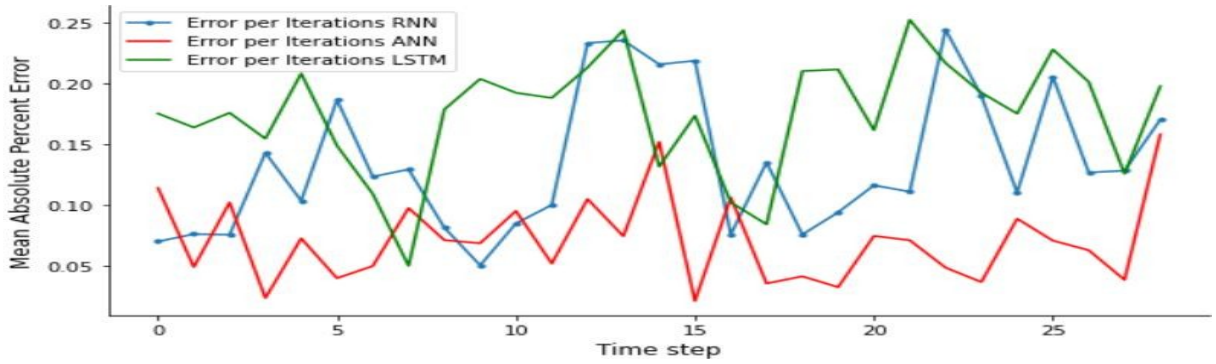

Figure 2. Error of different deep algorithms throw iterations.

Backward prediction using actual prediction with ANN, RNN and LSTM

In this section we are going to represent two algorithm of back-casting times series based on an Artificial Neural Network. We fix the hyper-parameters as follow:
20 epochs and 15 batch-size. We use Adam optimizer with a learning rate of 0.0065.

Algorithm 5.

1. Detection of the index of the first clean column t_0
2. Impute the hole missing values using Linear regression and consider this dataset as an input one.
3. Back-casting

$$Y_i = x_{l_0+1-i} = f_i\left(x_{l_0+2-i}, x_{l_0+3-i}, \ldots, x_N\right)$$

4. Use an ANN model Mi(n) related to each iteration and n would be the dimension of the input vector $X=\left(x_{l_0+2-i}, x_{l_0+3-i}, \ldots, x_N\right)$, then $n=2+i+N-l_0$, $\forall i = 3,\ldots,l_0$

4. At the end of the iteration, we calculate the predicted value.

$$Xx_{l_0+1-i} = ff_i\left(x_{l_0+2-i}, x_{l_0+3-i}, \ldots, x_N\right)$$

and we fix,

$$X_{l_0+1-i} = Xx_{l_0+1-i}$$

5. We calculate the error between this dataset and the already exact one.

At the end of the iterations, we are predicting a composition of approximation so the final prediction at the iteration 29 would be $FF_{29} = ff_{29} \circ ff_{28} \circ \ldots \circ ff_1$.
Here 29 corresponds to the total number of iterations.

Remark 5. In this algorithm each approximated predicted result replaces the last column of the old dataset and would be considered as an input for the next iteration. In this way the data would be more and more noisy from an iteration to the other and we expect that the error would increase through iterations but would be stabilized at less than 35% as it's illustrated in the Figure 3.
This is the figure of Mean Absolute Percentage error throw iterations which vary from 8% to 35% for all deep learning algorithms.

ISSN: 2961-6611

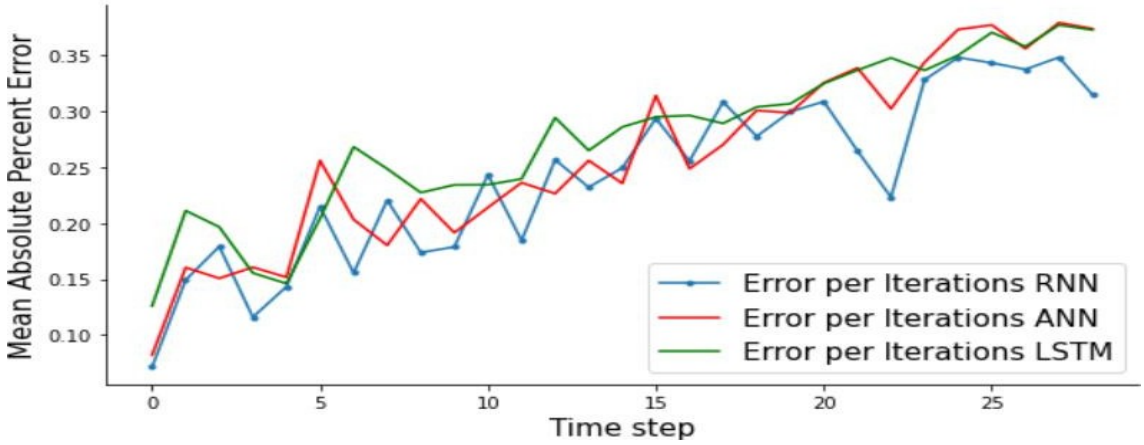

Figure 3 Error of different deep algorithms throw iterations.

Backward prediction with ANN, RNN and LSTM without the use of the exact database

In this section we are going to represent two algorithm of back-casting times series based on an Artificial Neural Network.

We start by the following neural network model by fixing the epochs at 20 and the batch size at 46.

Algorithm 6.

1. Detection of the index of the first clean column l0 of missing data.
2. Impute the hole missing values using Linear regression and consider this dataset as an input one.
3. Back-casting

$$Y_i = x_{l0+1-i} = f_i\left(x_{l0+2-i}, x_{l0+3-i}, \ldots, x_N\right) \ \forall i = 3,\ldots,l_0$$

4. Use an ANN, RNN and LSTM models Mi(n) successively related to each iteration and n would be the dimension of the input vector $X=\left(x_{l0+2-i}, x_{l0+3-i}, \ldots, x_N\right)$, then $n=2+i+N-l_0$, $\forall i = 3,\ldots,l_0$.
5. At the end of the iteration we calculate the predicted value

$$Xx_{l0+1-i} = ff_i\left(x_{l0+2-i}, x_{l0+3-i}, \ldots, x_N\right)$$

and we fix,

$$X_{l0-i} = Xx_{l0+1-i} \ \forall i = 3, .., l_0$$

6. At the end of the iterations we obtain the predicted dataset.
7. We calculate the error between this dataset and the already exact one. In reality in each iteration, we are determining the new column ˜f such that:

$$XX_{l0-i} = ff_{i+1}\left(ff_i\left(x_{l0+2-i}, x_{l0+3-i}, \ldots, x_N\right), x_{l0+2-i}, x_{l0+3-i}, \ldots, x_N\right)$$
$$\forall i = 3,..,,l_0$$

Remark 6. In this algorithm each approximated predicted result replaces the next missing column of the old dataset and would be considered as Y exact value for the next iteration. There is similarities between this technic and LOCF [9] (last observed carried forward) but our predicted observation is considered a more noisy one then it could approximates better the reality.

To test the accuracy of this approach we calculate the mean absolute percentage error with other classic imputation algorithms which could be considered as a quasi-exact data since from the beginning these algorithms are used to impute just less than 23% of the entire dataset.

These errors of accuracy are summarized in the following Table 1.

Even the algorithms seem reducing error from an iteration to another but it's approaching a totally predicted value then its reducing error with an inexact value that's why the error seems kind important compared with the exact values. Even this approximation seems less accurate than the preceding ones but in this approach we haven't at any step consider the existence of the complete dataset. So the originality of this work is even if we have not the exact dataset we can build afford acceptable predictions.

Table 1

Mean Absolute percentage error	ANN, RNN and LSTM without the use of the exact database		
	ANN	**RNN**	**LSTM**
Mean Imputation	37.9%	35.8%	31.5%
Linear Regression	39.2%	36.9%	33.6%
Linear Interpolation	40.6%	37..8%	38.2%
Spline Interpolation	42.7%	39.8%	39.2%

This is the Figure 4 of Mean Absolute Percentage error of prediction throw iterations which vary from 8% to 35% for all deep learning algorithms.

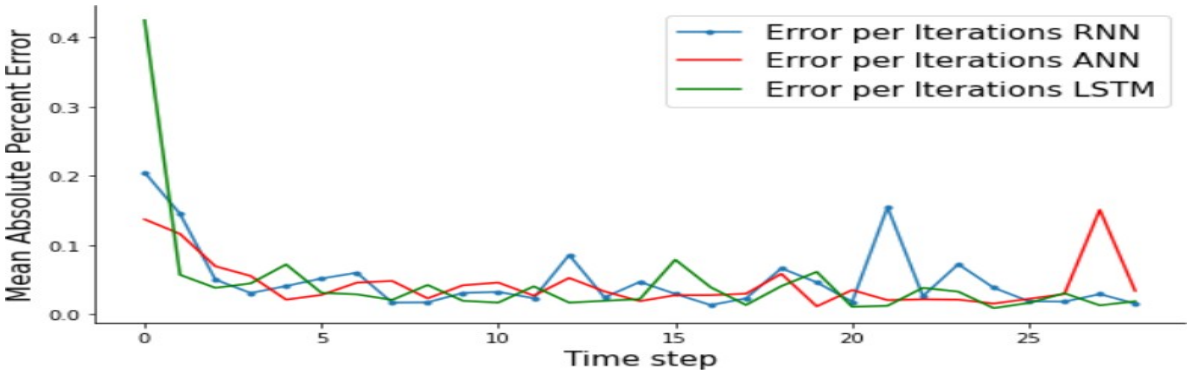

Figure 4. Error of different deep algorithms throw iterations.

Conclusion:

In this work we performed a deep learning algorithm: ANN, RNN and LSTM, not just only for imputation but categorically for reconstruction of missing values of all the nations and for the previous thirty years. We proposed a reconstruction sometimes based on a complete dataset of reference and also an unsupervised learning and without having a complete database of reference for training. Certainly in this work we deal with special distribution of missing value, the values are missing at the beginning of the time series so a backward prediction would be more accurate, if it was the opposite a forward prediction would occur and if the missing data were randomly distributed we must certainly search a relation between the missing values and then reconstruction of some of them would be synonym of a total reconstruction. These two last cases could be fixed as a future work. Another challenge occurs, certainly even we deal with a normalized indicator, but this times the linear interpolation at the last dense was able to give good approximation but sometimes it would be the case so a sigmoid use on the last dense is able to gives better results. All these technics could be fixed and treated as a future work.

References

[1] James D Hamilton. Time series analysis. Princeton university press, 2020.

ISSN: 2961-6611

[2] Firuz Kamalov. Forecasting significant stock price changes using neural networks. Neural Computing and Applications, 32(23):17655–17667, 2020.

[3] Neeraj Bokde, Marcus W Beck, Francisco Martínez Álvarez, and Kishore Kulat. A novel imputation methodology for time series based on pattern sequence forecasting. Pattern recognition letters, 116:88–96, 2018

[4] Konstantinos Benidis, Syama Sundar Rangapuram, Valentin Flunkert, Yuyang Wang, Danielle Maddix, Caner Turkmen, Jan Gasthaus, Michael Bohlke-Schneider, David Salinas, Lorenzo Stella, et al.

[5] Jason Hickel. The sustainable development index: Measuring the ecological efficiency of human development in the anthropocene. Ecological economics, 167:106331, 2020.

[6] Ahmed Tealab, Hesham Hefny, and Amr Badr. Forecasting of nonlinear time series using ann. Future Computing and Informatics Journal, 2(1):39–47, 2017

[7] Alaa Sagheer and Mostafa Kotb. Time series forecasting of petroleum production using deep lstm recurrent networks. Neurocomputing, 323:203–213, 2019

[8] Alper Tokgöz and Gözde Ünal. A rnn based time series approach for forecasting turkish electricity load. In 2018 26th Signal processing and communications applications conference (SIU), pages 1–4. IEEE, 2018

[9] Steffen Moritz, Alexis Sardá, Thomas Bartz-Beielstein, Martin Zaefferer, and Jörg Stork. Comparison of different methods for univariate time series imputation in r. arXiv preprint arXiv:1510.03924, 2015

ISSN: 2961-6611

Thermal Performance Assessment of an Atypical Trombe Wall Construction for A Mediterranean Area

Marwa AMMAR[#1], Ameni MOKNI[*2], Nahed SOUSSI[#3]

[#123]*Laboratory of Thermal and Thermodynamic of Industrial Processes,*
National School of Engineers of Monastir,
road of Ouardanine, 5000 Monastir, Tunisia
[1]ammarmriwa@gmail.com

***Abstract*— The Trombe Wall is a passive heating system designed for use in buildings to improve thermal conditions during low winter temperatures. The Trombe Wall is an affordable and easily integrated building feature. However, to make it more appealing and encourage its use in architecture, improvements are needed in both performance and aesthetics. This includes better solar building integration. To improve thermal comfort in buildings in the Mediterranean region, a modified Trombe Wall with a transparent sloping roof and transparent side walls containing slats of transparent insulation material is suggested. This research project analyses and compares the performance of a room with a traditional Trombe Wall and with the innovative Trombe Wall (T-T-W with TIM-PS) in improving thermal comfort. The new design improves thermal performance of heating from 5 to 35% at 5 p.m. Engineers and architects can integrate this new Trombe wall design into existing and new buildings to improve the building's energy performance.**

***Keywords*— Trombe Wall; ANSYS FLUENT, TIM, Thermal Performance, Winter Solstice Day**

I. INTRODUCTION

The Mediterranean region has the climate of the temperate regions, more often subtropical, that mark the land areas bordering the Mediterranean Sea. The average characteristics of the various Mediterranean climates are as follows: a rhythm of four well-contrasting seasons; a hot, dry summer; a marked but mild winter (the monthly average is never below 0°C); a spring and autumn that are sometimes very rainy, with a clear advantage in autumn. The Mediterranean climate, however harmonious it may be, remains one of the most threatened by climate change and the effects of pollution, which are forcing major meteorological revolutions.

The notion of thermal comfort is obviously the priority that comes to people's minds when they talk about the comfort of a building. Being warm and comfortable in winter, but not too hot in summer, while keeping energy consumption to a minimum: that's the challenge of thermal comfort in a sustainable building, which goes far beyond simple temperature regulation.

Buildings account for around 40% of the world's energy consumption. A large proportion of this energy is used to ensure thermal comfort in buildings [1]. A review of the literature on the indoor environment showed that thermal comfort, compared with visual and acoustic comfort and indoor air quality, is considered more important by building occupants [1]. However, when it comes to green buildings, actual energy consumption can be up to 2.5 times higher than predicted, due to the unpredictable nature of occupant behaviour and poor energy management [2]. More sustainable energy strategies, policies and systems are needed by promoting energy saving and efficiency. Sustainable construction and thermal comfort in buildings are currently the focus of researchers' attention.

It is very important and crucial to focus on optimizing energy efficiency in the building sector. To meet the new challenges of urban renewal in this century, it is essential to help local authorities and industry develop construction and innovation projects.

In this respect, the central question we could ask ourselves is the following: ***How can we ensure thermal comfort in buildings while respecting the principles of sustainable development?***

By relying on expensive heating methods that have a high impact on energy consumption, and on poor insulation that is incapable of preventing the transfer of cold inside the house, the houses built in our Mediterranean region

ISSN: 2961-6611

have low energy efficiency. Clearly, the parameters of climate, solar radiation, insulation, lighting, wind direction, etc. are ignored during the design phase. This is due to the fact that energy efficiency and bioclimatisation are still poorly covered in education and training programs. As our interest is in developing a range of innovations to ensure that buildings in the Mediterranean region provide better thermal comfort; the 3 pillars of sustainable development: the environmental, social and economic dimensions must be taken into account simultaneously. Optimizing the use of renewable systems and adopting appropriate strategies for the use of daylight to ensure new efficient buildings that can deliver consistently low energy requirements. A Trombe Wall is a powerful green feature of architecture supporting the ventilating, heating and cooling of buildings **[3]**. The Trombe wall solution has the potential to reduce energy bills for heating and, if properly implemented, its impact on the summer operation of the building must also be taken into account. Nevertheless, implementation of such a solution remains restricted, notably in hot climates, as there can be serious problems of indoor overheating even after the cooling period. Initially designed exclusively for the passive heating of buildings in continental climates, they have recently come under particular scrutiny because of their low cost, the simplicity of their installation geometry and their reliability of operation in other climatic contexts **[4]**. The ventilation openings and the operation of the shading device have a very appreciable impact on the fluctuation of temperatures in a Trombe Wall; these parameters were studied experimentally by A.Briga-Sá et al.**[5]**, under the real climatic conditions of a Portuguese city.

In Tunisia, they were analysed in **[6]**, in which the comparison between a numerical model and experimental data for a single-zone building showed that the installation of 3 m^2 of Trombe wall reduced the heating demand by 28% compared with a traditional wall. But currently the Trombe wall concept has not yet been implemented into Tunisian buildings. And F.Abbassi et al. **[7]** have investigated four types of building materials, namely concrete, stone, brick, and adobe, for energy and economic reasons to identify the optimal thickness of Trombe Walls. Based on the energy data collected from TRNSYS software, the most suitable material choices that can contribute to a 50% reduction in heating loads for a single room appear to be stone and concrete. In particular, the calculations indicate a thickness of 34 cm for stone and 32 cm for concrete, with a payback period of 2.85 years and 2.65 years for concrete.

We are proposing in this work an urban architectural design innovation that will ensure better thermal comfort in winter and summer. This involves reducing as far as possible the consumption of electricity from fossil fuels for the purposes of thermal comfort within the building, and exploiting solar energy to the maximum. It's all done while respecting the compromise between high productivity and low cost. To successfully integrate passive solutions, the architecture of the building must be correctly defined in the preliminary design phase. This means adapting the shape and configuration of the building to maximise the use of renewable energy sources, such as solar radiation, and using passive devices in line with the bioclimatic architecture approach.

Taking into account the architectural aesthetics and integration principles of solar buildings, this article proposes a new concept for building façades, which will represent a real technological and aesthetic innovation in architectural design, involves familiarizing ourselves with the "Trombe Wall" concept aimed at ensuring thermal comfort throughout the seasons.

In this study, which differs from similar works, the new design of the Trombe wall comprises a sloping roof that is highly transparent to the sun's rays, combined with side walls made transparent to the radiation. Thermal performance was increased by enlarging the area of solar radiation collection while reducing heat transfer to the external environment thanks to the inclusion of transparent slats made of transparent insulation material, while maintaining low cost and the most attractive architectural design.

II. . MATHEMATICAL THEORY AND GOVERNING EQUATIONS

- Continuity equation

$$\frac{\partial u_i}{\partial x_i} = 0 \qquad [1]$$

- Momentum equation

$$\frac{\partial \rho u_i}{\partial t} + \frac{\partial u_j \rho u_i}{\partial x_j} = -\frac{\partial p}{\partial x_i} + \frac{\partial}{\partial x_j}\mu\frac{\partial u_i}{\partial x_j} - \rho g_i \beta (T - T_0) \qquad [2]$$

- Energy equation

$$\frac{\partial \rho C_p T}{\partial t} + \frac{\partial u_j \rho C_p T}{\partial x_j} = \frac{\partial}{\partial x_j} K \frac{\partial T}{\partial x_j} + q \qquad [3]$$

ISSN: 2961-6611

III. NEW DESIGN OF TROMBE WALL

The experimental lightweight construction is achieved by building a wooden room oriented to the south. The measurements of the wooden room are 3 m (length) × 3 m (width) × 2.8 m (height), i.e. approximately 9 m^2 of usable area and 25 $m^3$of volume. The side facing south is made of 6 mm thick clear glazing and a 70 mm thick wooden panel, leaving an air space measuring 400 mm. It is necessary to completely isolate the room; for this reason, the interior of the wooden piece is covered with Styropor insulation. The southern side dimensions of the building being 3 m wide and 2.7 m high. It consists of 9 glass panes measuring 900 mm * 850 mm. Standard Trombe Walls are only able to perceive solar radiation for a given south direction, whereas the novel design of the Trombe Wall assumes that the lateral facades of the wall and the above roof have been replaced by glass. The side faces of the Trombe Wall consist of two glass surfaces measuring 1.3*0.3 m^2 each.

TIM parallel slats are joined to the southern glass cover. They are attached to the glass covering and positioned so that they do not touch the massif wall.

In the numerical component, temperature and flow evaluations of two different Trombe wall designs were performed based on experimentally verified Trombe wall dimensions. A 3D model was created in ANSYS FLUENT 16.1 and used to perform the Trombe wall analysis.

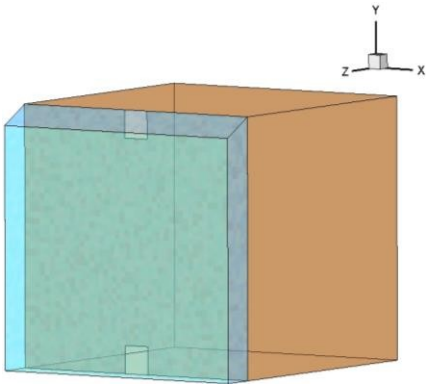

Fig.1:3D Model of the Transparent Trombe Wall

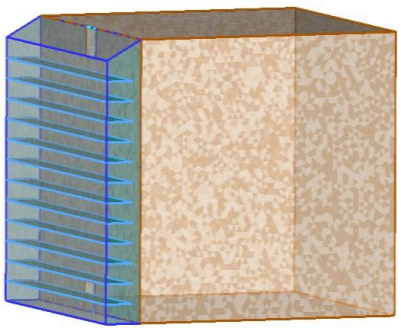

Fig.2: Transparent Trombe Wall with TIM-PS

IV. RESULTS AND DISCUSSION

3D numerical calculations performed using the SIMPLE algorithm volume control method quantify the heat transfer by free convection that occurs in the channel of a new and original Transparent Trombe Wall system. Estimating the thermal performance of the façade is the main task of evaluating the Trombe Wall façade. The study was carried out on the basis of average absorbed solar heat, and the results show that increasing efficiency was one of the main issues addressed during the optimised design of the new Trombe Wall.

ISSN: 2961-6611

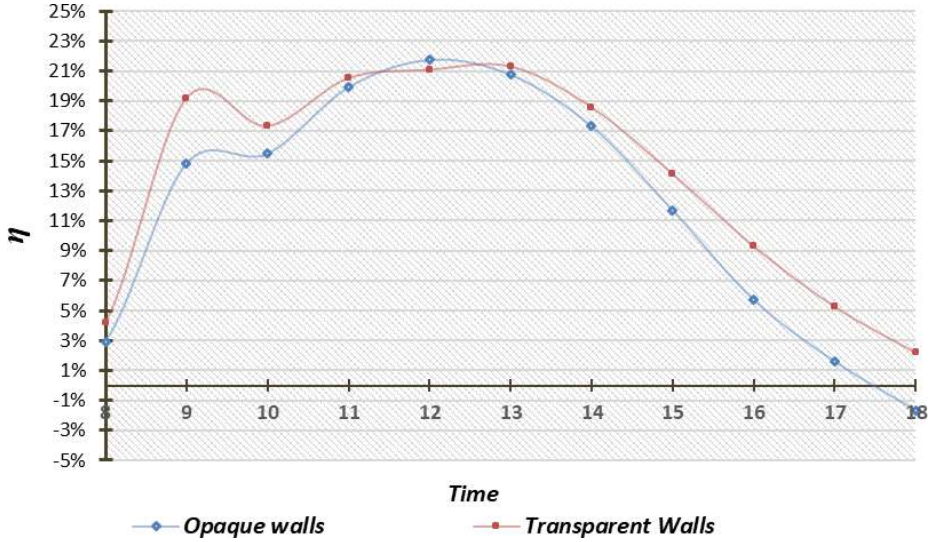

Fig.3: Thermal Efficiency of Transparent Trombe Wall unit with transparent and opaque's lateral walls and roof for a winter solstice day

Details of the thermal performance of the Trombe Wall unit with transparent and opaque's lateral walls and roof were collected based on the temperatures entering and leaving the room, and plotted in Fig.3. The findings reveal that the contribution of solar radiation to thermal efficiency remains clear, and is often the cause of significant convective heat loss. This passive heating system heats rooms using solar energy. It is important to note that the highest thermal performance of the Trombe wall is that of the transparent Trombe Wall, which is obviously due to the higher solar energy values received at the surfaces.

In this system, solar radiation hits the external sloping glazing on the roof, the side walls and the south face of the glass wall, heating the solid wall and the air contained in the space between the glass and the wall. the heat is transmitted by air convection and radiation from the solid wall to the interior of the room, resulting in an increase in temperature and, consequently, improved thermal comfort. The increase in transparent glazed surfaces allows greater heat transmission to the interior of the building and a significant improvement in thermal comfort. It can be appreciated that the traditional scenario has the lowest efficiency during the hours of the day except midday, when the classic Trombe wall with opaque wallS performs better, which is obviously due to the higher heat losses caused by the enlargement of the transparent glazed surfaces.

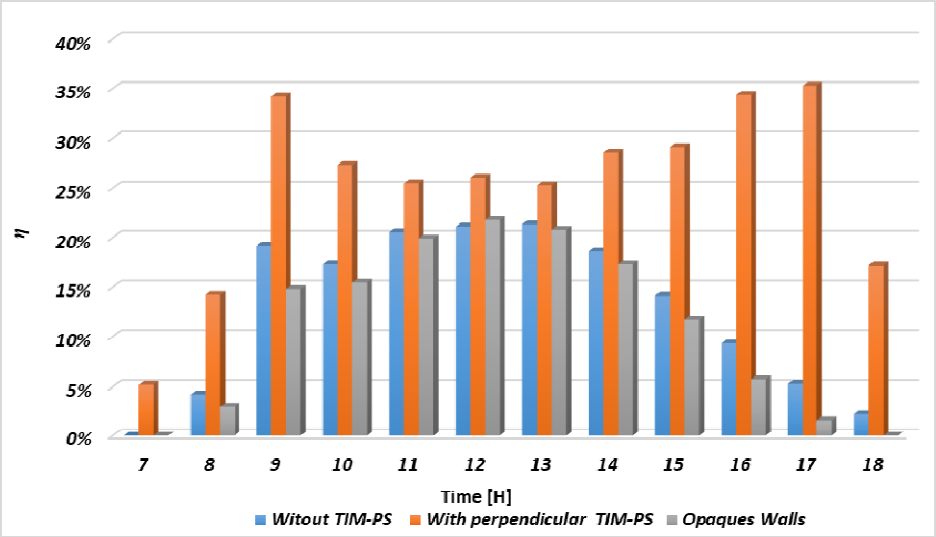

Fig.4: Thermal Efficiency for TIM-PS and Conventional Transparent Trombe Wall

ISSN: 2961-6611

The initial results of Fig.4 show that the new Trombe Wall can generate heating for up to 12 hours with a minimum efficiency of around 5%, compared to only 9 hours with a conventional Trombe Wall. This improvement is achieved by fitting the perpendicular glass wall with TIM-PS. The TIM-PS encourage the movement of the thermisiphon; however, the most likely cause of this efficiency gain is the limitation of convection losses through the TIM-PS. This prevents convection from the Trombe wall to the glazing, which occurs when the temperature of the wall is higher than that of the glazing (during the extreme hours of the day). Operational efficiency is considered to be linearly dependent on (Tin - Tout), as a consequence of the heat loss coefficient, so it has been observed that perpendicular TIM-PS reduce heat loss and therefore increase thermal efficiency.

V. CONCLUSIONS

The research provides valuable insights into sustainable building design and energy-efficient solutions in Mediterranean contexts. The new design of the Trombe wall has proved to be a great advantage in terms of improving thermal efficiency, since it has improved the thermal performance of the heating from 5 to 35% at 5 p.m. The new design can easily provide heating for 12 hours a day on a typical winter's day, making it highly appropriate for fitting into office architecture.

REFERENCES

[1] Liu Yang, Haiyan Yan, Joseph C. Lam, Thermal comfort and building energy consumption implications – A review, Applied Energy, Volume 115, 15 February 2014, Pages 164-173

[2] Guofeng Qiang , Shu Tang , Jianli Hao , Luigi DiSarno , Guangdong Wu , Shaoxing Ren , Building automation systems for energy and comfort management in green buildings: A critical review and future direction, journal/renewable-and-sustainable-energy-reviews" Reviews Volume 179, June 2023, 113301

[3] S. Duan, C. Jing, and Z. Zhao, “Energy and exergy analysis of different Trombe walls,” Energy and Buildings, vol. 126, pp. 517–523, 2016, doi: 10.1016/j.enbuild.2016.04.052.

[4] Piero Piero Bevilacqua, Federica Benevento, Roberto Bruno, Natale Arcuri, Are Trombe walls suitable passive systems for the reduction of the yearly building energy requirements?, Energy (2019), doi: 10.1016/j.energy.2019.07.003

[5] A. Briga Sá, J. Boaventura-Cunha, J. C. Lanzinha, and A. Paiva, “An experimental analysis of the Trombe Wall temperature fluctuations for high range climate conditions: Influence of ventilation openings and shading devices,” *Energy and Buildings*, vol. 138, pp. 546–558, 2017, doi: 10.1016/j.enbuild.2016.12.085.

[6] Abbassi F, Dimassi N, Dehmani L. Energetic study of a Trombe wall system under different Tunisian building configurations. Energy Build 2014. doi:10.1016/j.enbuild.2014.05.036.

[7] F. Abbassi, N. Naili, and L. Dehmani, “Optimum Trombe Wall thickness in the Mediterranean Tunisian context: An energetic and economic study,” Energy Science and Engineering, vol. 10, no. 8, pp. 2930–2939, 2022, doi: 10.1002/ese3.1179.

ISSN: 2961-6611

Comparative Analysis of Hand Sanitizers: A Simplified Approach Using FTIR Spectroscopy

Wafa MEJRI-BELGAIED [a,b],Henda JEMNI[a] , Borhen ABID[a] and Jamel-Eddine BELGAIED [b]

a. National Drug Control Laboratory of Tunisia, Jebel Lakhdar Street, 1006 Bab Saadoun-Tunis, Tunisia

b. University of Carthage, National Institute for Applied Science and Technology, INSAT, Ecochimie Laboratoiry (LR21ES02),. B.P. 676, 1080 Tunis Cedex, Tunisia

Email 1 wafabelgaied78@yahoo.fr

Email 2 jemni_hind@yahoo.com

Email 3 borhene2005@yahoo.fr

Abstract **A simple, selective, linear and accurate Fourier transform infrared (FTIR) spectroscopy method for the determination of ethanol and isopropanol in Hand sanitizers was developed. This method was compared to the Gas Chromatography with FID method used traditionally for the determination of ethanol and isopropanol. The developed method was further validated according to the International Conference on Harmonization guideline Q2 (R1). The developed method is linear over the concentration range of 40 to 100%. It was successfully applied for quality control of several hand sanitizers commercialized in Tunisia**

Keywords— sanitizer, ethanol, isopropanol, gas chromatography, Fourier transform infrared spectroscopy

I. INTRODUCTION

The Coronavirus Disease-2019 (COVID-19) outbreak is an unprecedented global pandemic, sparking grave public health emergencies. One of the measures to reduce COVID-19 transmissions recommended by the World Health Organization is hand hygiene, i.e., washing hands with soap and water or disinfecting them using an alcohol-based hand sanitizer (ABHS). Unfortunately, competing ABHSs with unknown quality, safety, and efficacy thrived, posing yet another risk to consumers [1]. Traditionally, gas chromatography (GC) with FID detection is used, but it is expensive and time-consuming [2, 3]. This study proposes an alternative approach based on Fourier transform infrared (FTIR) spectroscopy for HS analysis.

II. MATERIALS AND METHODS

An Agilent 8890 GC system (Agilent Technologies, USA) consisting of a Flame Ionisation Detector FID, a Nitrogen Phosphorus Detector, an auto sampler, an EPC headspace(G4556A) and a multi-mode Inlet (G3540A) with a Teknokroma capillary GC column (30m × 0,32 mm; 3 µm) was used.

For the FTIR system a Shimadzu Fourier Transform Infrared Spectrophotometer FTIR SPIRIT-IR was used.

The GC Head Space method consists of:

Column	Material: fused silica; dimensions: l = 30 m, Ø = 0.53 mm; Stationary phase: cyanopropyl (3) phenyl(3) methyl (94) polysiloxane R (film thickness 3 µm). Carrier gas: nitrogen for chromatography R
Flow rate	3 mL/min.
Split ratio	1:50
Static head-space conditions used:	equilibration temperature: 85 °C equilibration time: 20 min.
Detection	Flame ionisation

The following temperature program was used:

	Time(min)	Temperature (°C)
Column	0-1.6 1.6-9.9 9.9-13.6 13.6-20	40 40-65 65-175 175
Injection port	-	200
Detector	-	200

ISSN: 2961-6611

The FTIR Spectroscopy method is based on the quantification of characteristic bands for ethanol (ν_C-O: ~ 1045 cm^{-1}) and isopropanol (ν_C-O: ~ 1130 cm^{-1}). Both methods were validated according to ICH Q2 (R1).
The statistical analysis was performed using Statgraphics Plus software, version 4.0

III. Results and Discussion

Both methods were used for the determination of ethanol and isopropanol content in several Hand Sanitizers commercialized in Tunisia (ten samples containing Ethanol and ten samples containing Isopropanol).

The chromatogram below shows the Ethanol pic given by the GC system (retention time ~ 10.5 min)

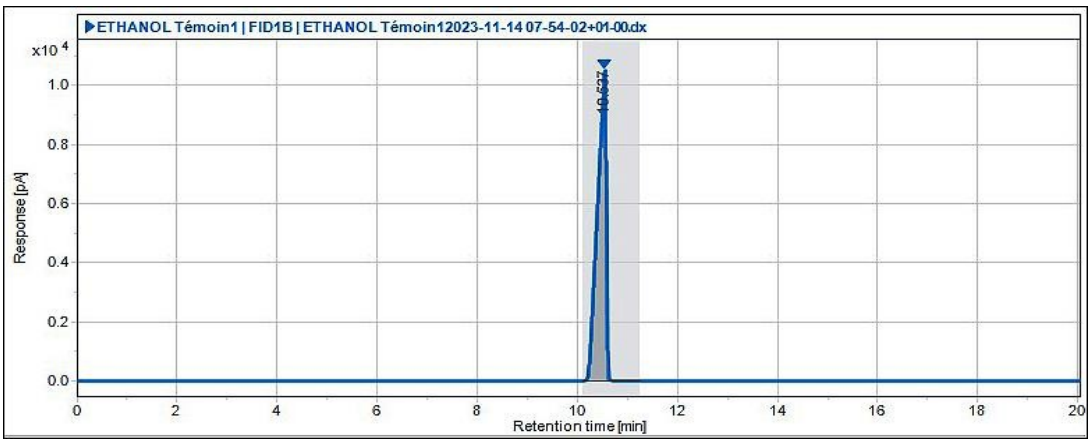

Fig. 1:chromatogram of Ethanol

The Infrared spectrum shows the characteristic band for ethanol (ν_C-O: ~ 1045 cm^{-1})

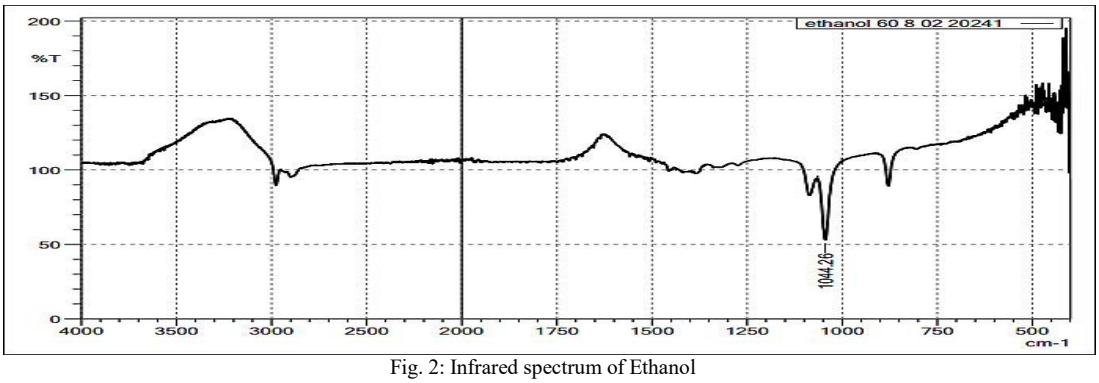

Fig. 2: Infrared spectrum of Ethanol

The results found for the ethanol content are detailed in the following table:

	Results found with GC method (%)	Results found with FTIR method (%)
1	73.5	74.0
2	63.4	63.5
3	70.2	71.0
4	87.9	87.0
5	75.0	75.2
6	68.5	68.0
7	50.2	50.0
8	60.5	61.0
9	55.5	55.0
10	75.0	75.0

ISSN: 2961-6611

Table 1:Ethanol content(V/V) in Hand sanitizers

Both methods present the same results regarding the Ethanol proportion in the different samples.
The chromatogram below shows the Isopropanol pic given by the GC system (retention time ~ 11.5 min)

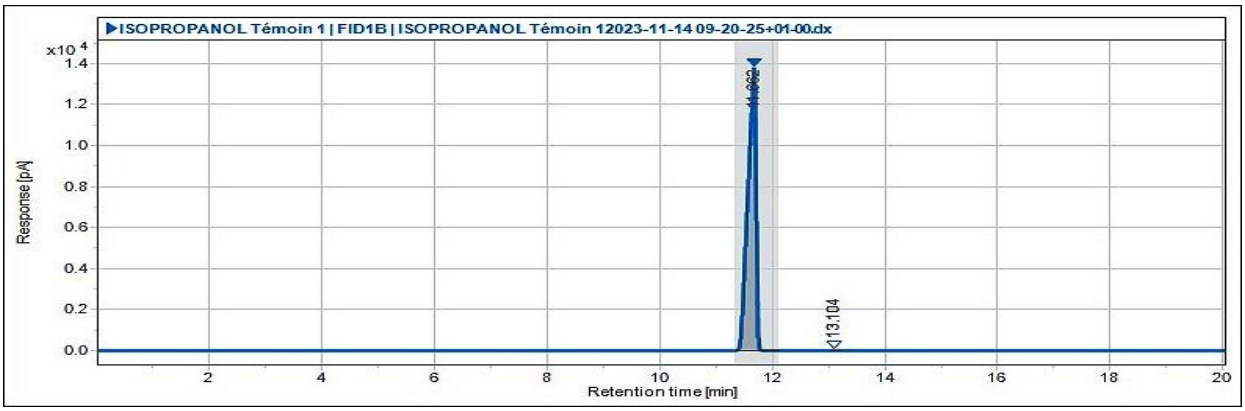

Fig. 3: chromatogram of Isopropanol

The Infrared spectrum shows the characteristic band for Isopropanol (ν_C-O: ~ 1130 cm^{-1})

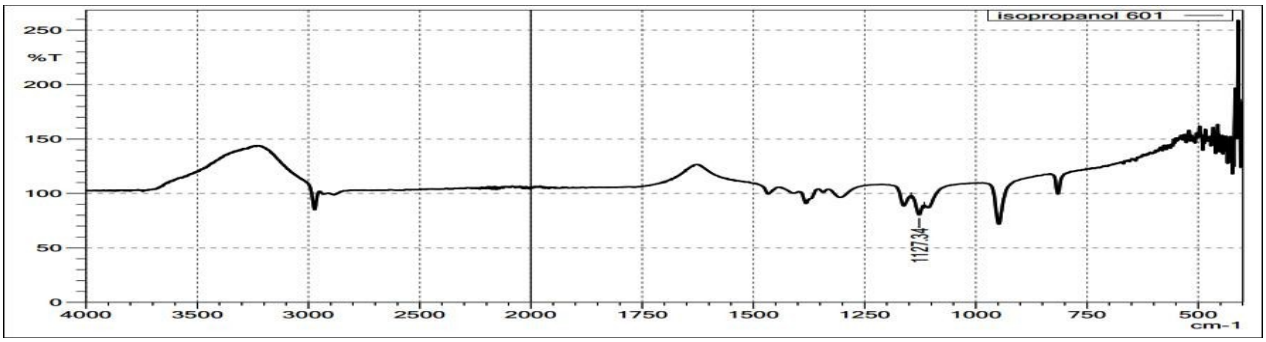

Fig. 4 Infrared spectrum of Isopropanol

The results found for the Isopropanol content are detailed in the following table:

	Results found with GC method (%)	Results found with FTIR method (%)
1	52	52.5
2	64.5	63.5
3	54.5	54
4	62	62
5	60.5	60
6	57.5	57.0
7	55.5	55.0
8	50.5	51.0
9	60.2	60.0
10	54.5	54.5

Table 2:Isopropanol content in Hand sanitizers

Both methods present the same results regarding the isopropanol proportion in the different samples.

ISSN: 2961-6611

The CPG and FTIR methods were validated according to ICH Q2 (R1). We found that both were specific, accurate, linear over the concentration range of 40 to 100 %. The correlation coefficient found for the linearity test was 0.999. The obtained recoveries were in the [98.22-99.32] range. Precision was assessed with respect to both repeatability and intermediate precision. Results were expressed in terms of relative standard deviation (% RSD) and found to be less than 2 % indicating excellent precision

IV-CONCLUSION

FTIR spectroscopy provides a simple, rapid, and cost-effective alternative to GC for HS analysis. It allows for quick and precise determination of ethanol and isopropanol concentrations, providing vital information for HSs quality control and safety. This method represents a significant advancement in HSs analysis, reducing the cost, time, and complexity of analysis.

REFERENCES

[1] P. Matatiele et al. Scientific Reports | (2022) 12:4231.
[2] L. Muleba et al. Int J Environ Res Public Health. 2022 Aug; 19(15): 9245
[3]. D. W. Lachenmeier, Side Effects of Drugs Annual, 2021.

ISSN: 2961-6611

TiO_2-SnO_2:F coupled oxide thin films for photocatalytic applications: Enhancement of photodegradation of organic pollutants

Wafa Naffouti* and Najoua Turki-Kamoun
Laboratoire de Physique de la Matière Condensée, Faculté des Sciences de Tunis, Université de Tunis El Manar, Tunisie (2092), Tunisia.
*Email Adress – wafanaffouti19@gmail.com

***Abstract* - TiO_2-SnO_2:F mixed oxide thin films have been deposited on glass substrates, using spray pyrolysis technique. The aim of this investigation is to study the effect of sprayed solution concentration of both TiO_2 and SnO_2:F oxides on structural (by XRD), optical (by Spectrophotometery) and spectral (by spectrofluorimetry) properties of TiO_2-SnO_2:F coupled oxide thin layers. In fact, X-ray diffraction analysis revealed that all coupled oxides exhibited the formation of both anatase phase of TiO_2 material and tetragonal structure of SnO_2:F compound. Optical properties depicted a high transmission in the visible range and an energy band gap in the order of 3.75 eV. Photoluminescence (PL) spectra displayed several emissions, in the visible region, indicating a diverse range of electronic transitions within the grown films. In order to evaluate photocatalytic activity, tests were conducted on TiO_2-SnO_2:F layer using both Malachite Green (MG) and Rhodamine B (RhB) pollutants. An efficiency of about 85 and 90 % was obtained for both MG and RhB, respectively.**

***Keywords* - TiO_2-SnO_2:F mixed oxide thin films, Spray pyrolysis method, photocatalytic activity, Malachite Green and Rhodamine B pollutants.**

I. INTRODUCTION

Coupled titanium and fluorine doped tin (TiO_2-SnO_2:F) oxide thin films are investigated in a large range of applications including gas sensing [1], antibacterial activity [2] and photocatalysis [3,4]. In fact, titanium dioxide material is popular in the field of pollutant degradation due to its high photocatalytic activity, capability to decompose and remove a wide variety of pollutants under UV light, good resistance to acid, low cost, good chemical stability and non toxicity. Despite these benefits, there are some constraints such as the variation of structural form, low photon efficiency, a relatively high electron-hole recombination rate and the need of ultraviolet radiation for excitation. All these constraints may impact, negatively, the photocatalytic performance of TiO_2 compound. Thus, in order to address these limits, coupling with other metal oxides, such as SnO_2 [5], WO_3 [6] and ZnO [7], have been investigated. Among them, tin dioxide (SnO_2) compound plays an important role in the improvement of photocatalytic activity by generating more hydroxyl radicals.
Several synthetic routes have been employed in order to deposit TiO_2-SnO_2 mixed oxide thin films, including RF sputtering [8], pulsed laser deposition [9] and spray pyrolysis technique [10]. Among them, chemical spray pyrolysis method is cost effective, flexible, and allows the synthesis of large area of thin films with controlled conditions.
Thus, this investigation aims to synthesize TiO_2-SnO_2:F coupled oxide thin films using spray pyrolysis technique and to evaluate the photocatalytic performance of the grown layers.

II. EXPERIMENTAL DETAILS AND CHARACTERIZATION

TiO_2-SnO_2:F thin films have been deposited on glass substrates using spray pyrolysis technique. It consists on the pulverization of a transparent solution on heated glass substrates. In fact, TiO_2 and SnO_2:F solutions were prepared independently. Thus, TiO_2 solution was obtained by dissolving titanium tetraisopropoxide (TTIP: $C_{12}H_{28}O_4Ti$) and acetylacetonate (AcAc: $C_5H_8O_2$) in ethanol (C_2H_6O) [11]. Concerning SnO_2:F solution, it was achieved using $SnCl_4$, H_2O and methanol as precursors. Fluoride (NH_4F) has been added to SnO_2 solution in order to obtain the fluorine doping [12]. Both TiO_2 and SnO_2:F solutions were mixed with various contributions, while the total volume is kept constant and equals to 90 ml, as shown in Table 1. The films were grown at a substrate temperature and a flow rate of about 350 °C and 15 ml/min, respectively. The elaboration process was followed by an air annealing at 500 °C for 2 hours.

ISSN: 2961-6611

TABLE 1
SAMPLES' NOMINATION OF TiO_2-SnO_2:F MIXED OXIDE THIN FILMS.

Sprayed solution Volume (ml)	V_{TiO2} (ml)	$V_{SnO2:F}$ (ml)	Sample
90	90	0	TiO_2
	60	30	T60S30
	45	45	T45S45
	30	60	T30S60
	0	90	SnO_2:F

TiO_2-SnO_2:F thin layers cristallinity was performed using X-ray diffraction analysis (XRD) by XPERT-PRO diffractometer system in the range of 20 to 80°. The wavelength, current and accelerating voltage were in the order of 1.5418 Å, 30 mA and 40 kV, respectively. Optical properties were examined by means of UV-NIR spectrum with a Perkin-Elmer Lamda 950 spectrophotometer for wavelength in the range of [250-2000] nm. Photoluminescence (PL) spectra were recorded using a Perkin-Elmer LS55 Fluorescence spectrometer, at room temperature, with an excitation wavelength in the order of 300 nm.

The photocatalytic performance of TiO_2-SnO_2:F coupled oxide thin films has been evaluated by the photodegradation of both malachite green (MG) and Rhodamine B (RhB) organic pollutants. Thus, MG and RhB solution were prepared, in glass bottle, by dissolving both of them in bi-distilled water. The solution concentration was about 3.10^{-5} M for the two dyes. Then, the grown films were immersed into aqueous MG and RhB solutions. Then, after sun irradiation, the change of solutions' concentration, as a function of irradiation time (0.5, 1 and 2 h), was recorded using a spectrophotometer Perkin Elmer Lambda 950.

III. RESULTS

A. Structural Analysis

***Fig*.1** illustrates the XRD spectra of chemically sprayed TiO_2-SnO_2:F mixed oxide thin films deposited at various solution concentrations of TiO_2 and SnO_2:F oxides. As it can be observed, XRD spectra of pure and coupled oxides reveal a polycrystalline character. Indeed, several XRD peaks may be detected in pure TiO_2 spectrum. These peaks are located at around 2 θ = 25.27, 37.72 and 47.89° corresponding, respectively, to (101), (103) and (200) crystal planes. These peaks may be assigned to the anatase phase of TiO_2 compound according to JCPDS card N°89-4921, where (101) plane is the preferred orientation [13].

Tetragonal SnO_2:F crystal may be, also, identified with the presence of diffraction peaks located at around 26.49, 33.81, 37,98, 51.49 and 61.81° corresponding to (110), (101), (200), (211) and (310) reticular planes, where the (200) is the preferred orientation (JCPDS N° 46-1088).

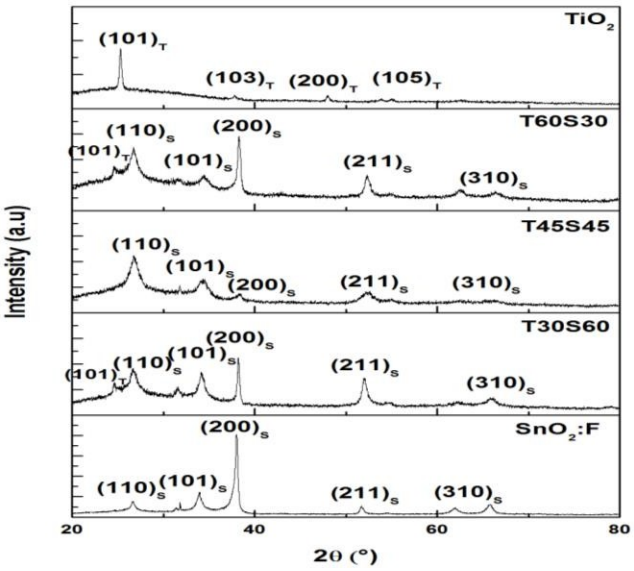

Fig. 1 XRD Spectra of chemically sprayed TiO_2-SnO_2:F thin films deposited at different oxides' contribution.

Furthermore, it is clear from ***Fig. 1*** that, in the case of coupled oxide samples, both anatase TiO_2 and tetragonal SnO_2 compounds may be identified. This finding proves that the growth of TiO_2-SnO_2:F mixed oxide has been, successfully, achieved. It is important to signal that tetragonal SnO_2:F crystal is dominant for T60S30 and T30S60

ISSN: 2961-6611

samples. However, there is, practically, an equal contribution of both TiO_2 and SnO_2:F compounds in the case of T45S45 sample.

B. Optical Analysis

Fig.2 depicts transmission ***(a)*** and reflexion ***(b)*** spectra of TiO_2-SnO_2:F thin layers grown on glass substrates at various oxides' contribution. In fact, for wavelength higher than 1000 nm, i.e. in the near infrared region, transmission values are in the range of 60 to 90 % for TiO_2, T60S30, T45S45 and T30S60 samples. However, it is found to decrease, drastically, in the case of SnO_2:F layer.

In the visible range, transmission value is, practically, about 80 % for all the samples, and it is found to decrease with SnO_2:F solution volume increment. Furthermore, one can remark the existence of interference fringes which indicates the homogeneity of the grown layers as well as the uniformity of the thickness.

Furthermore, it is important to signal that the transmission decreases, drastically, until cancelation in the vicinity of UV region, i.e. for wavelength in the range [280 – 370] nm. This behaviour corresponds to the absorption edge of TiO_2-SnO_2:F coupled oxide thin layers. This later is found to shift towards lower wavelengths with SnO_2:F solution volume increment indicating an increase of the band gap values as it will be discussed later.

Reflexion values ***(Fig.2.a)*** are found to be about 20 %, in the transparency region for all the samples.

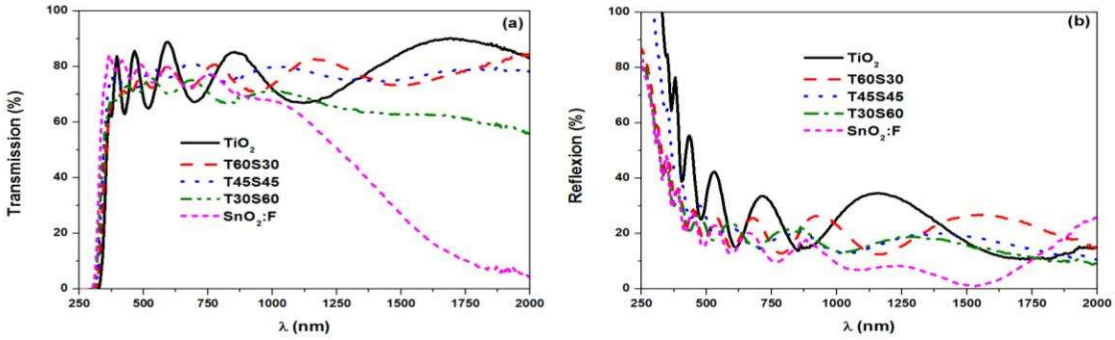

Fig.2 Transmission (a) and Reflexion (b) spectra of TiO_2-SnO_2:F thin layers deposited at different oxides' contribution.

For further optical investigation, optical band gap energy (Eg) has been determined basing on the differential transmission spectra (dT/dλ), as displayed in ***Fig. 3***. In fact, the peak with the highest intensity corresponds to the band gap energy of the compound [14].

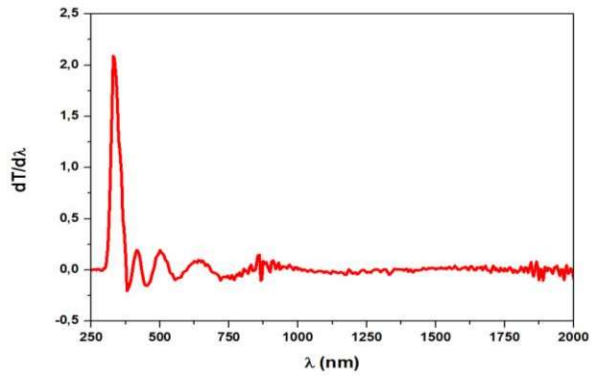

Fig. 3 The plot of dT/d λ versus λ of T45S45 sample.

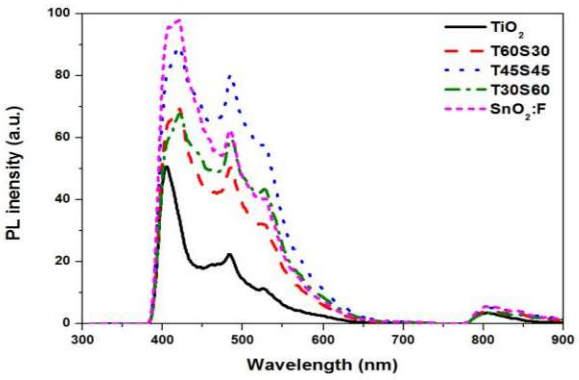

Fig. 4 PL spectra TiO_2-SnO_2:F thin layers.

The obtained results are summarized in ***Table 2***. It is found to increase, slightly, with SnO_2:F solution volume increment.

TABLE 2
BAND GAP ENERGY OF TiO_2-SnO_2:F MIXED OXIDE THIN FILMS

Sample	TiO_2	T30S60	T45S45	T30S60	SnO_2:F
Eg (eV)	3.49	3.76	3.75	3.70	3.75

Fig. 4 depicts photoluminescence (PL) spectra of chemically sprayed TiO_2-SnO_2:F thin layers grown at various oxides' contribution. Thus, one can notice that all PL spectra show several emissions in the visible region. These emissions indicate a diverse range of electronic transitions within the material, which can be influenced by factors such as impurities, defects, and changes in composition. By analysing these emissions, researchers can gain insights into the optical properties and electronic structure of the material, allowing them to understand its behavior under different conditions and optimize it for specific applications.

C. Photocatalytic Performance

ISSN: 2961-6611

Photocatalytic performance of T45S45 sample has been evaluated using both malachite green (MG) and Rhodamine B (RhB) organic pollutants. Therefore, ***Fig.5*** displays the temporal change of MG and RhB photodegradation for various sun irradiation times in the case of T45S45 sample. In fact, absorption spectrum, showing the change of aqueous pollutant solution, is very useful in order to evaluate the photocatalytic behavior of the catalysis. Thus, as it can be observed from ***Fig. 5***, there is an important decrease of the absorption peak of both MG and RhB dyes, located at 616 and 554 nm, respectively, with sun irradiation time increment. This finding proves the good degradation of the dyes using the photocatalysis, and, thus, an improvement of photocatalytic activity can be revealed. In fact, this behavior may be explained by the fact that both TiO_2 and SnO_2:F oxides have different Fermi levels as well as band gap energy. Thus, there is an enhancement of photo-generation as well as electron-hole separation [15]. Furthermore, as it can be seen, RhB concentration decreases faster compared to MG.

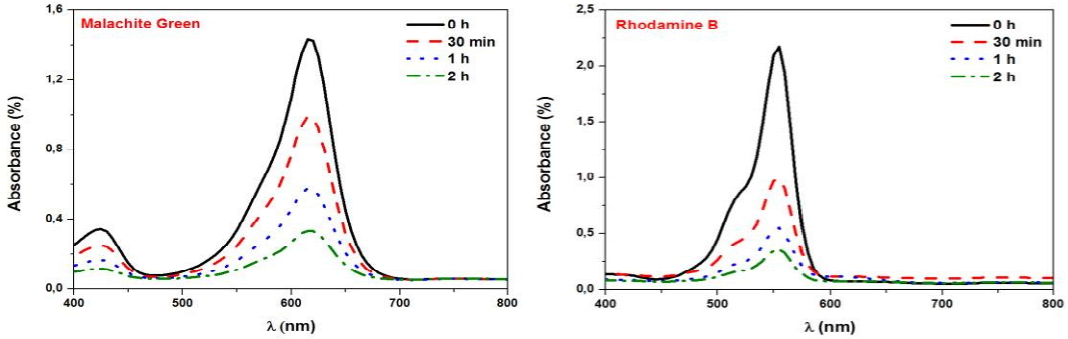

Fig. 5 Temporal change of MG and RhB photodegradation for various irradiation times for T45S45 sample.

The photocatalytic efficiency of MG and RhB dyes calculated using the following equation [15]:

$$Efficiency(\%) = \frac{C0 - C}{C0} * 100$$

The obtained results are depicted in ***Fig.6***. It is evident that the photodegradation efficiency reaches 85 and 90 % for both MG and RhB, respectively.

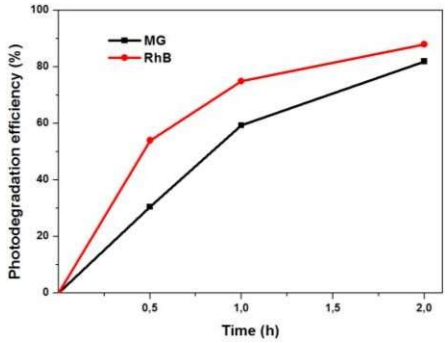

Fig.6 Photodegradation efficiency of MG and RhB for different sun light irradiation time for T45S45 sample.

IV. CONCLUSION

In summary, coupled oxide TiO_2-SnO_2:F layers have been grown on glass substrates using Spray pyrolysis technique at various oxides' contribution. Indeed, XRD analysis reveals the presence of both anatase TiO_2 and tetragonal SnO_2 materials. Furthermore, it is worth noting that the grown layers exhibit high optical transmission in the order of 80% with a band gap of about 3.75 eV. PL spectra illustrate various emissions in the visible range. Photocatalytic activity of T45S45 sample for both malachite green as well as Rhodamine B organic dye has been investigated and an efficiency of about 90% is found for sun irradiation time equals to two hours.

REFERENCES

[1] C. M. Carney, S. Yoo, S. A. Akbar, *Sensors and Actuators B: Chemical*, 108, 1–2, 29-33, 2005.
[2] Lek Sikong, Budsabakorn Kongreong, Duangporn kantachote, weerawan sutthisripok. 2(2010)120-125.
[3] K. Liu, X. Wu, B. Wang, Q. Liu, Mater. Res. Bull. 37 (2002) 2255–2262.
[4] J. Martinez, D.R. Acosta, G. Cedillo, Thin Solid Films 490 (2005) 118–123.
[5] Carmen M. Carney, Sehoon Yoo, Sheikh A. Akbar, Sensors and Actuators B 108 (2005) 29–33.
[6] H. Dhiflaoui , K. Khlifi, L. A. Ben Cheikh, Surface and Coatings Technology, Volume 326, Part A, 15 October 2017, Pages 45-52.

ISSN: 2961-6611

[7] P. Larios, R. Lopez, A. Hernández Gordillo, F. Tzompantzi, R. Gómez, L.M. Torres-Guerra, Fuel, Volume 100, October 2012, Pages 139-143.
[8] K. Zakrzewska, M. Radecka, Thin Solid Films 515 (2007) 8332–8338.
[9] S. Rashed, A. Haider, S. Younis, Part B Eng. Technol. J, 2014.
[10] N. Manjula, K. Kaviyarasu, A. Ayeshamariam, G. Selvan, A. Diallo, G. Ramalingam, S. Mohamed, D. Letsholathebe, M. Jayachandran, Journal of Nanoelectronics and Optoelectronics, Volume 13, Number 10, 2018, pp. 1543-1551(9).
[11] Hussin RO, Choy KL, Hou XH. Advanced Materials Research. 2016 Feb 2;1133:352-6.
[12] M. Ajili, M. Castagné, N. Kamoun-Turki, Optik, 126 (2015) 708-714.
[13] W. Naffouti, T. Ben Nasr, A. Mehdi, N. Kamoun-Turki. Effect of sprayed solution flow rate on the physical properties of anatase TiO 2 thin films. Journal of electronic materials. 2014 Nov;43:4033-40.
[14] N. Houaidji, M. Ajili, B. Chouial, N.T. Kamoun, Optik. 208 (2020), 164026.
[15] Sibhatu AK, Weldegebrieal GK, Sagadevan S, Tran NN, Hessel V. Chemosphere. 2022 Aug 1;300:134623.

ISSN: 2961-6611

AI-Enhanced Bionic Leg

Achref Soua[#1], Bilel Charfi [*2], Mohamed Hedi Riahi[#3]

[#]*ESPRIT school of engineering*
1, PôleTechnologique, 2 Rue André Ampère Ariana 2083
Email 1 - achref.soua@esprit.tn
Email 2 - bilel.charfi@Esprit.tn
Email 3 – mohamedhedi.riahi@esprit.tn

Abstract:

This workdelvesinto the development of a next-generationbionic leg thatleveragesartificial intelligence (AI) and deeplearning for enhancedfunctionality. Traditionalprosthetics, whilefunctional, lackedadaptability. This paperaddressesthis limitation by integratingcutting-edge technologies. The bionic leg utilizesadvancedsensor data, signal processing, and an electric jack to achievesuperiorsensitivity and terrain adaptability. The report willanalyzethese innovative components, compare them to conventional solutions, and showcase the advancementsachieved. By exploring the synergybetween AI and biomechanics, thisresearch paves the way for future advancements in human-machine collaboration.

Key words : artificialintelligence, bionic leg, deeplearning, data, biomechanics

1-Introduction :

For centuries, prosthetics have played a pivotal role in the realm of medicine. Transitioningfrom basic attachments to sophisticatedbiomechanical solutions, traditionalprostheticlimbs, whilefunctional, oftenfell short in adapting to the evolvingneeds of amputees. Recognizing the limitations of thesemedical interventions, numerousstudies have been initiated to enhance the naturalness, adaptability, and efficiency of prosthetics. Bionic legs enhanced by artificial intelligence (AI) have emerged at the intersection of advancements in prosthetics and AI. The concept of fusingthesetwodomains has gained traction in recentdecades, spurred by technologicalprogressthat has unlockednovelpossibilities. Prostheticsboast a richhistory, stretching back to antiquitywithrudimentary prototypes. Throughout the centuries, they have undergone transformations driven by the adoption of more sophisticatedmaterials and manufacturingtechnologies[1,2,3,7]. The rise of AI has ushered in innovative perspectives acrossvariousfields, prostheticsincluded. The integration of AI has the potential to elevate the functionality of artificiallimbs, rendering them more adaptable and intelligent. A significantbreakthrough has been the advent of myoelectricprostheses, leveraging the detection of electricalsignalsfromresidual muscles to governmovement. This development has paved the way for the real-time integration of AI for control and adjustment. Pioneeringresearch initiatives and

ISSN: 2961-6611

projectshave delvedinto the synergies between AI and prosthetics, laying the groundwork for the realization of AI-poweredbionic legs.Over the pastdecade, significant strides in leg prosthetics have surpassedmere imitation of human motion, extendingtowards the realm of potentialenhancement. This researchintroduces the development of an advancedbionic leg incorporatingartificial intelligence (AI) and deeplearningalgorithms. Leveraging sophisticatedsensor data and employing signal processing techniques, this state-of-the-art bionic leg showcases heightenedsensitivity and adaptability[4,5,6,7]. To furtherenrichitscapabilities, weintroduce the integration of an electric jack, enablingadjustments and robust support across diverse terrains and activities. Our methodologyencompasses the design of a distinctive solution, featuring key technicalcomponents:

- Real-time reading and processing of gait data through a sensor network comprisingtwo IMU sensors, robustmathematicalfilters, and denoisingautoencodersis crucial to minimizesensorerrors and elevate data quality.

- Treatment of time-series data usingsequence-to-value mechanismsenhancesourcomprehension of the temporal nuances in humangait, enablingprecisepredictions of knee angles at optimal moments.

- Prediction of knee angles throughrobust machine learning and deeplearningmodelsfacilitates efficient communication of accurate angles to the electric jack, aidingamputees in the effortless performance of dailyactivities.

- Optimization of predictionprecision and latencythroughTensorFlow Lite encoding and C++.

- Implementation of a self-learningenvironment by recording patient data, allowing model retraining for betteralignmentwithindividualamputees.

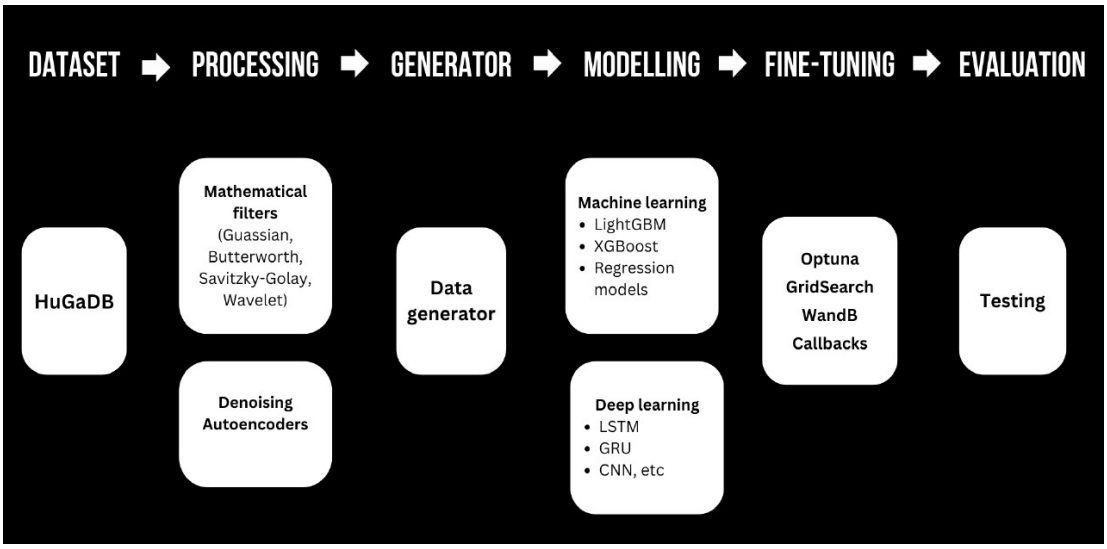

ISSN: 2961-6611

Our proposed solution constitutes a comprehensive pipeline, covering data reading, cleaning, knee angle prediction, and inference. This innovation ispoised to have a profound social impact on amputees, facilitating the seamless and effortlessexecution of theirdailyactivities.

2-Data understanding

This section emphasizes the crucial role of biomechanics, particularlyknee joint angles, in creating a robustdataset for AI-poweredprosthetics. By understanding the intricatemovements of humangait, includingknee flexion and extension, researchers can gatheraccurate data essential for developing intelligent prosthetics. This section delvesinto the biomechanics of humangait, focusing on the significance of the knee angle in data collection and ultimately, achievingour goal of a more advanced AI prosthetic.

2-1-Locomotion and gait cycle

This section lays the groundwork for understanding data collection in the development of AI-poweredprosthetics. It introduces the concept of locomotion, the science behindbodilymovement, with a specific focus on the lower body mechanicsinvolved in walking. The humangait cycle, a fundamental process in locomotion, isthenexplained. This cycle consists of two key phases: stance (foot on the ground) and swing (foot in the air). A figure (not included in thistext format) isreferenced to illustratethese phases. By understandingthese aspects of humanmovement, researchers can effectivelycollect data necessary for creating a more advanced AI prosthetic.

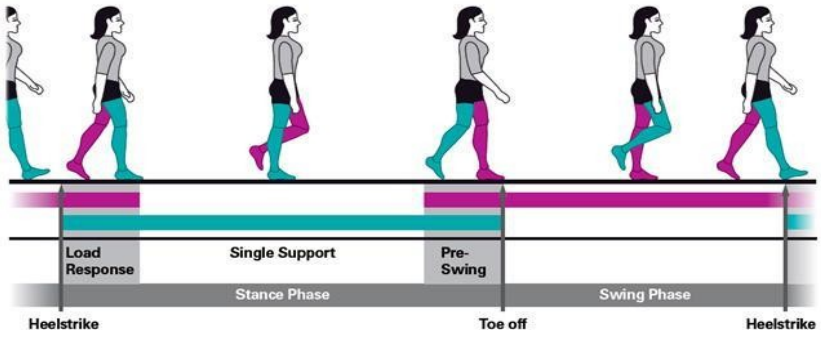

Figure 1: The swing and stance during a gait cycle

2-2- Knee angle

Nowthatwe'vegrasped the intricacies of human locomotion and the gaitcycle's dual phases, it's time to delveinto the behavior of the human leg during motion, particularlyfocusing on the knee and itsdynamic angle changes.

Throughout the gait cycle, the knee angle undergoes variations to accommodate the diverse walking phases. During the stance phase, the knee angle diminishes (flexes) as the leg supports the body'sweight, facilitatingforwardmovement over the foot. Conversely,

ISSN: 2961-6611

during the swing phase, the knee angle increases (extends) to enable the leg to swing forward .What'smostintriguing about thisphenomenonis the consistent pattern observed in the plot of knee angle per gait cycle—a distinctive shapefeaturing one brief peak and one elongatedpeak, as depicted in the figure below.

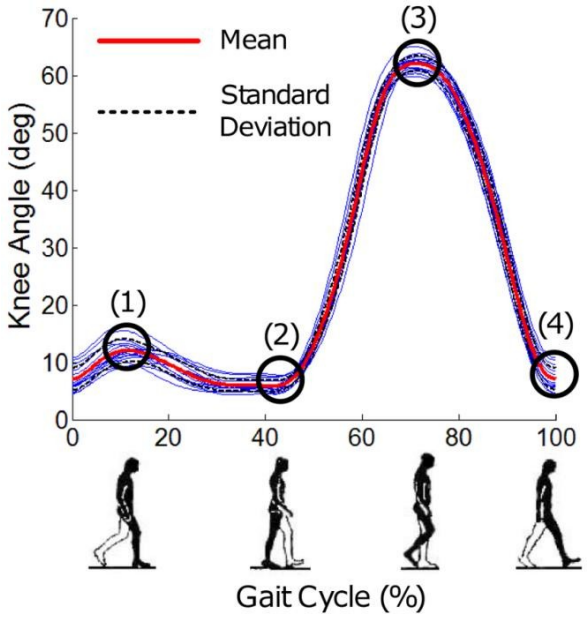

Figure 2:Knee angle per gait cycle

2-3- Relationship betweenknee angle and the shin and thigh

In order to capture significant data that can tell us about the knee angle, the science of locomotion and physics states thatthereis a strongrelationshipbetweenacceleration and rotation in a 3D space, from the thigh (above the knee) to the shin (below the knee) on and around the 3-axis X, Y, and Z. This relationship has a direct impact on the value of the knee angle, which ranges from 0 to 140 degrees.

As a matter of fact, thesevectors can beused to estimate the rotation around a certain axis, as explained in the figure below.

ISSN: 2961-6611

$$\theta = \tan^{-1}\left(\frac{\Delta y}{\Delta x}\right)$$

θ = ATAN2(YT - YS, XT - XS)

WHERE:

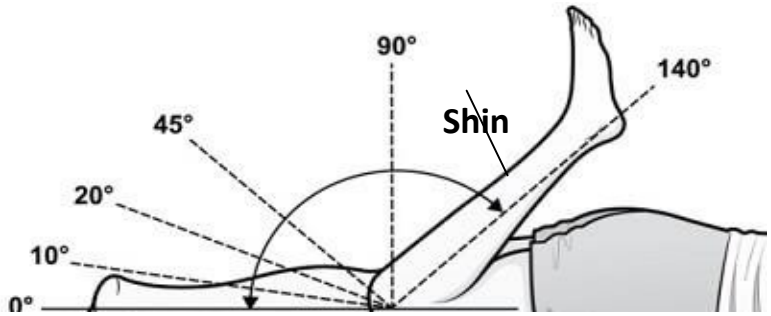

Figure 3:Knee angle estimation based on acceleration of the shin and thigh

This studyhelps us understand the relevance of usingacceleration and rotation of the shin and thigheach, on the X, Y, and Z axis, thisconcludesour primal features.
In order to capture the acceleration and rotation of the shin and thigh, weproposed the usage of inertialmeasurementunits (IMU) whichwewill talk about in detail in the next section.

3- Data collection

In order to collectour data, whichis a time series of acceleration and rotation on both the shin and thigh, weproposed the use of sensors, in particular, inertialmeasurementunits (IMU).

3-1- Inertialmeasurement unit (IMU)

An inertialmeasurement unit, commonlyreferred to as an IMU, is an advancedelectronicdevicethat has a collection of sensors, generally an accelerometer to measureacceleration on a 3-axis, a gyroscope to capture the rotation around the 3-axis, and a magnetometer to record the magneticfield.

In ourresearch, accelerometers are used to detect changes in linear motion and changes, which translate to how a limb moves forward, sideways, or verticallyduring a walking motion. By measuringaccelerations on three orthogonal axes (X, Y, and Z), the accelerometerprovides a three-dimensionalview of the movement.[1]

On the other hand, gyroscopes measureangularvelocity. This becomes pivotal whenanalyzingcomplexhumanmovementswhere the orientation of a limb changes as it moves.

ISSN: 2961-6611

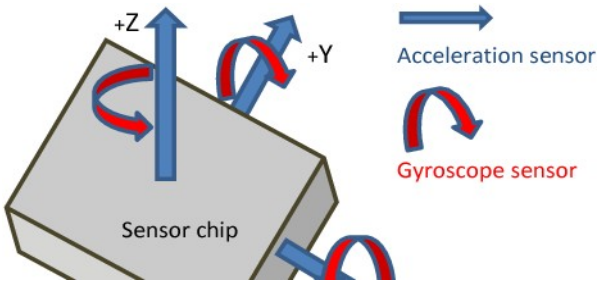

Figure 4:IMUs axis and orientation

3-2- IMU position on the leg during data collection

As mentioned in the previous section, both the shin and thigh have important roles in humangait, althoughtheirdynamics and motions are waydifferent, thisis due to the factthat the thighismuchcloser to the humanbody's mass center, it's main roleis to control the forward motion. On the other hand, the shinis more distal, soits main mission is to adjust to the ground and surface variations and maintain balance.

The perfect position for the inertialmeasurementunits (IMU) is to beplacedapproximately on the center of the thigharound 5 centimetersabove the knee, depending on the height of the subject. The sameapproachis for the second IMU [1,9], as itneeds to bepositioned 5 centimetersbelow the knee on the center of the shin, exactly as shown in the figure below.

ISSN: 2961-6611

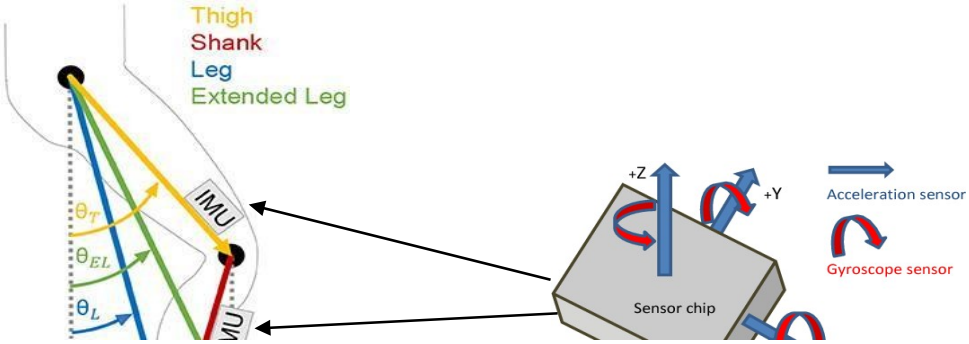

Figure 5: Gyroscope and accelerometer placements

3-3-Dataset and features

Aftergaining insights into the humangait and kneebehaviorduringmovement, as well as understanding the significance of capturingthigh and shinacceleration and angularvelocity, it's time to explore ourdataset, itsfeatures, and key characteristics. However, beforedelvinginto the dataset, it's essential to discussour data collection trial and the options weconsidered.

a) Manual Data Collection

Sensor data collection is a laborious process requiring a team of experts, substantial hardware, and a diverse subject pool. Eachrecording session is time-consuming, and hardware malfunctions or sensorerrors are commonrisks. In our case, limitedresourcesposedchallenges—wehadonly one micro cardwith one IMU and a team of twoengineers. This constraint made gathering a large datasetseemdaunting, especiallyconsideringthateachrecording session needed to berepeated for both the shin and thigh. Ultimately, wemanaged to collectonly 20 recordings, eachcapturing 10 to 20 seconds of one subjectwalking. Additionally, weencountered issues withsensor grip on the body, leading to movement and displacementduringsubject motion. Thesecircumstancesprompted us to seek an alternative approach to continue ourresearch[1,9].

b) The Open-Source Dataset:HuGaDB

To address the challengesmentioned, wesought an open-source database meeting specificcriteria. The datasetneeded to be extensive to train robustdeeplearningmodels, collectedusing a definedprotocol (sensor type and positioning on the human body), and include a diverse subject

ISSN: 2961-6611

pool. Our searchled us to HuGaDB, or Human GaitDatabase, whichfulfilled all ourcriteria, except for one crucial aspect—the absence of knee angle values. However, HuGaDBcontainedsensor data collectedfrom 18 subjectsperformingvariousactivitiessuch as walking, standing, and running.

To address the missingknee angle values, weopted to calculateprecise estimations for eachmeasurement. Whilethisposed a significantsetback, ourlimitedresourcesnecessitated a solution-orientedapproach. Wedecided to employsensor fusion techniques to estimateknee angles accurately[1,9].

4-Techniques for data preprocessing and signal denoising

Data, in itsrawform, can bemisleading due to the noise itcontains, aftercarefulstudy and processing, itwill have a greatpotential to help ourresearchsucceed. As we dive into the techniques of data refinement, ourprimary objective is to ensure the clarity and reliability of ourdataset. This chapterpresents an overview of the methodsdeployed, segmentedintothree main categories:

4-1- Classicpreprocessing

Beforegoingthroughadvancedfiltering techniques, itwasimperative to addressfundamental data irregularities, and the classingpreprocessingsteps.

Handling NaN Values: As a preliminarystep, wescannedourdataset for any NaN (Not a Number) values, ensuringthat for suchinconsistencies, wehad no Nan values. This gives us the green light for the nextstep

OutlierDetection and Correction: A notable irregularity in ourdatasetwas the gyroscope readings, which, in certain instances, wereamplifiedtenfold. This ismentioned in the official paperpublished by the owners of the HuGaDBdatabase. Throughoutlierdetection techniques, these anomalies wereidentified and rectified by dividing the values by 10.

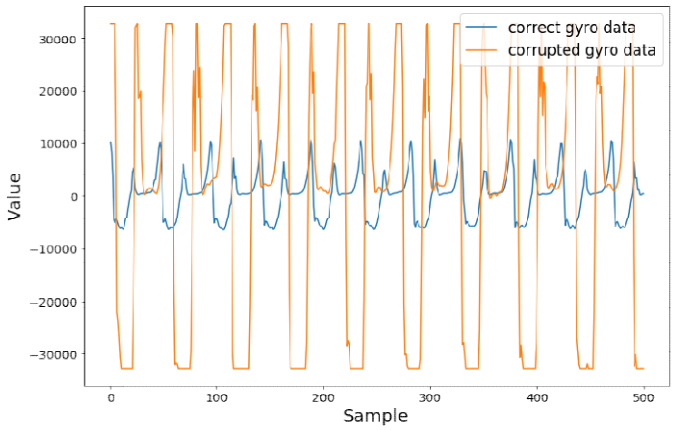

Figure 6:Corrupted vs. correct gyroscope values

ISSN: 2961-6611

4-2- MathematicalFilters

Aftertackling the classicmethods, it's time to move on to the appropriatemethods for signal processing and denoising like mathematicalfilters. Thesemathematicalfunctions serve as essential tools to extract pertinent signalsfrom a noisy background. Our task in this phase is to try and test variousfilters to decidewhich one is more suitable for our data and researchsubject.
Weexperimentedwith a variety of filters:Kalman, Wavelet, Butterworth, Gaussian, Median, High-Pass, Low-Pass, movingaverage, and Savitzky-Golay, tweakingparameters for optimal results[5,6,7,8,9,10,11].

Kalmanfilter[1]: As discussed in the previouschapter, a recursivealgorithmthat can beused to estimate the state of a dynamic system from a series of noisymeasurements.

x_hat(t+1) = x_hat(t) + K(t) * (z(t) - H(t) * x_hat(t))
where:

x_hat(t) is the estimate of the state of the system at time step t
K(t) is the Kalman gain matrix at time step t
z(t) is the measurement at time step t
H(t) is the measurement matrix at time step t

Waveletfilter:is a signal processing technique that uses functionsnamedwavelets to remove noise from a signal. Wavelets are mathematicalfunctionsthat can beused to decompose a signal into a series of basis functions. The basis functions are chosensuchthatthey can represent the signal withdifferentlevels of detail.

The main steps of a waveletfilterare:

Choose a wavelet
Decompose the signal intowavelet coefficients using the discretewavelettransform (DWT) or the fast wavelettransform (FWT).
Threshold the wavelet coefficients using the soft thresholdingmethod or the hard thresholdingmethod.
Reconstruct the denoised signal by combining the thresholdedwavelet coefficients using the inverse wavelettransform (IDWT) or the inverse fast wavelettransform (IFWT).

ISSN: 2961-6611

$$W(a, b) = \int x(-t)\, \psi(a-1t-b)\, dt$$

where:

W(a, b) is the wavelet coefficient at scale a and translation b
x(t) is the signal
ψ(t) is the waveletfunction

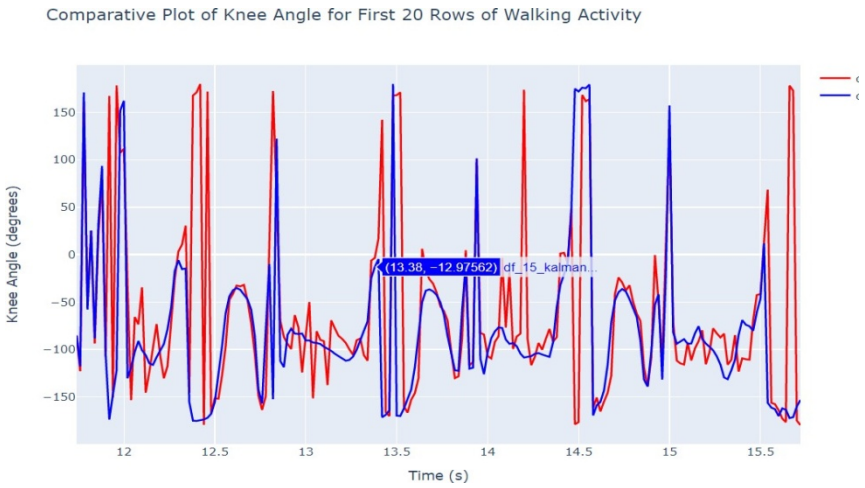

Figure 7: Original vs denoised data usingWaveletfilter

Butterworthfilter:is a type of low-passfilterthatiswidelyused in signal processing. It isknown for its flat frequencyresponse in the passband and itssharpcutoff in the stopband. This makesthemideal for applications such as denoisingsignals and filtering out unwantedfrequencies.

$$H(s) = 1 / (1 + (s/\omega\_c)^2n)$$

where:

H(s) is the transferfunction of the filter
sis the complexfrequency
ω_cis the cutofffrequency of the filter
nis the order of the filter

ISSN: 2961-6611

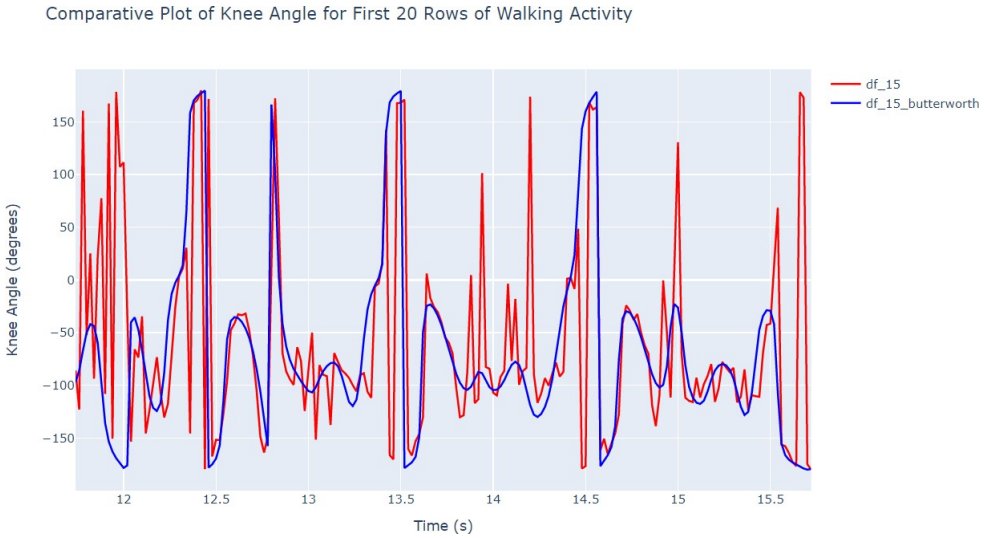

Figure 8: Original vs denoised data usingButterworthfilter

Gaussianfilter:is a type of filterthat uses Gaussianfunctionswhich are functions are bell-shapedcurvesthat are symmetricalaroundtheirmean. They are alsoknown as normal distributions.

$$H(x, y) = \exp(-(x^2 + y^2) / 2\sigma^2)$$

where:

H(x, y) is the value of the filter at pixel (x, y)
σis the standard deviation of the Gaussianfunctio

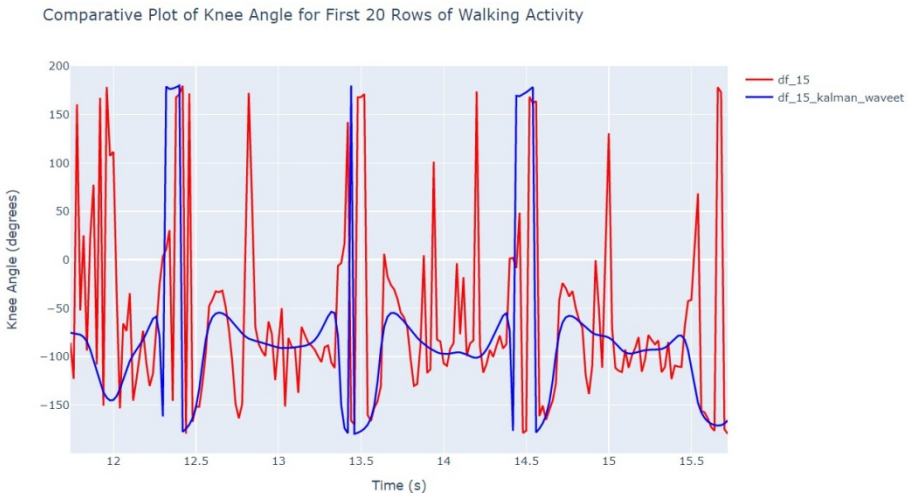

Figure 9: Original vs denoised data usingGaussianfilter

Medianfilter[2]: thisis a type of filterthat uses the median value of a neighborhood of pixels to replace the value of the central pixel. The median value is the middle value in a

ISSN: 2961-6611

sortedlist of values. It iscommonlyused in image processing but can beused in certain cases in signal treatment.

y(x, y) = median(x(x, y - k), ..., x(x, y + k), x(x - k, y), ..., x(x + k, y))
where:

y(x, y) is the output pixel value at (x, y)
x(x, y) is the input pixel value at (x, y)
kis the radius of the filter

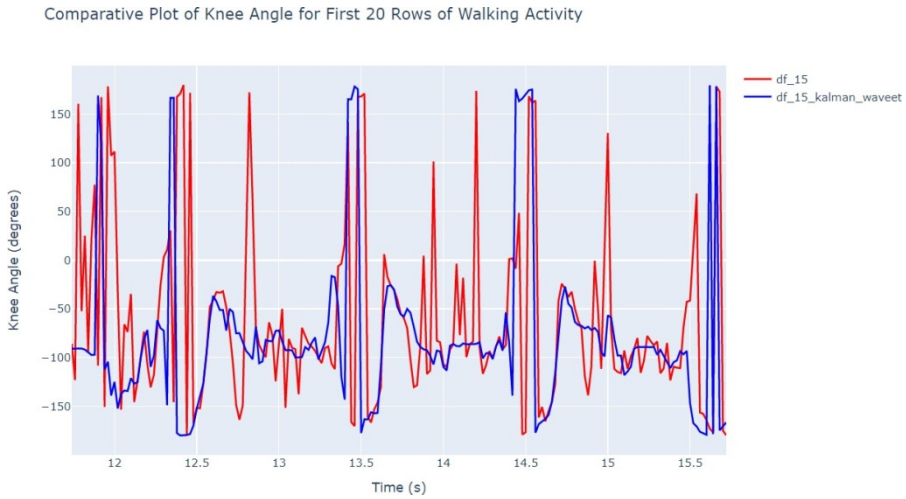

Figure 10: Original vs denoised data usingMedianfilter

Low-passfilter[3]: is a filterthat passes signalsbelow a certain frequency, known as the cutofffrequency, and attenuatessignalsabove the cutofffrequency. Low-passfilters are used in a variety of applications, including signal processing, image processing, and control systems.

H(s) = 1 / (1 + sRC)
where:

H(s) is the transferfunction of the filter
sis the complexfrequency
R is the resistance of the filter
C is the capacitance of the filter

High-passfilter[4]: opposite to the low-passfilter, itis a filterthat passes signalsabove a certain frequency, known as the cutofffrequency, and attenuatessignalsbelow the cutofffrequency.

ISSN: 2961-6611

H(s) = sC / (1 + sRC)

where:

H(s) is the transferfunction of the filter
sis the complexfrequency
R is the resistance of the filter
C is the capacitance of the filter

Savitzky-Golay filter[5]: is a digital filterthat can beused to smooth data and differentiate the data. It is a non-recursivefilter, whichmeansthatitdoes not use feedback to calculate the output. This filterworks by fitting a polynomial to a window of data points. The polynomial isthenevaluated at the center of the window to produce the output value. The window size and the order of the polynomial are parameters of the filter.

$$y[i] = \sum_{j=-(n-1)/2}^{(n-1)/2} a_j * x[i + j]$$

where:

y[i] is the output value at index i
x[i] is the input value at index i
nis the window size
a_j are the filter coefficients

Moving averagefilter[6]: is a type of digital filterthatsmooths data by replacingeach data point with the average of a set of nearby data points. The number of data points in the set iscalled the window size.

$$y[i] = 1/w * \sum_{j=-(w-1)/2}^{(w-1)/2} x[i + j]$$

where:

y[i] is the output value at index i
x[i] is the input value at index i
wis the window size

ISSN: 2961-6611

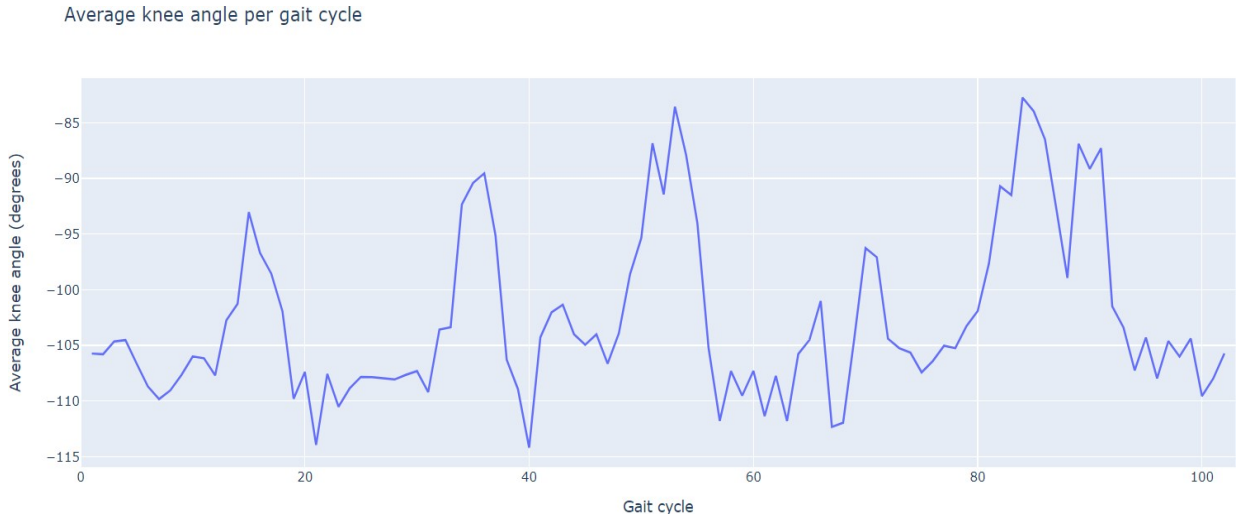

Figure 11: Moving averagefiltereffect on data

After extensive evaluations, twofiltersemerged as the front-runners: the Low-Passfilter and Savitzky-Golay. Theirefficiency in isolating relevant gait data, combinedwith light computationalrequirements, renderedthem the best choices.

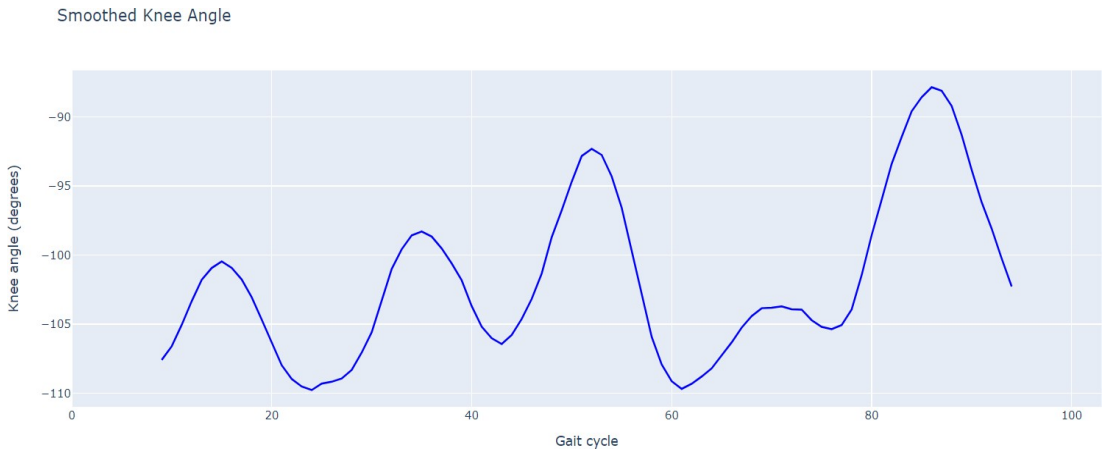

Figure 12: Original vs. denoised data usingSavitzky-Golay and Low-passfilter

4-3- Denoisingautoencoder

Denoisingautoencoders[7] are a type of neural network that can beused to remove noise from data. They are a powerfultoolthatworks by learning to reconstruct the original data from a noisy version of the data.

Denoisingautoencoders are typicallydesigned as twoseparate neural networks: an encoder and a decoder. The encoder takes the noisy data as input and producesembedded, vectors, alsoknown as latent representations of the data. The

ISSN: 2961-6611

decodertakes the latent representations as input and produces a reconstruction of the original data[5,6,7].

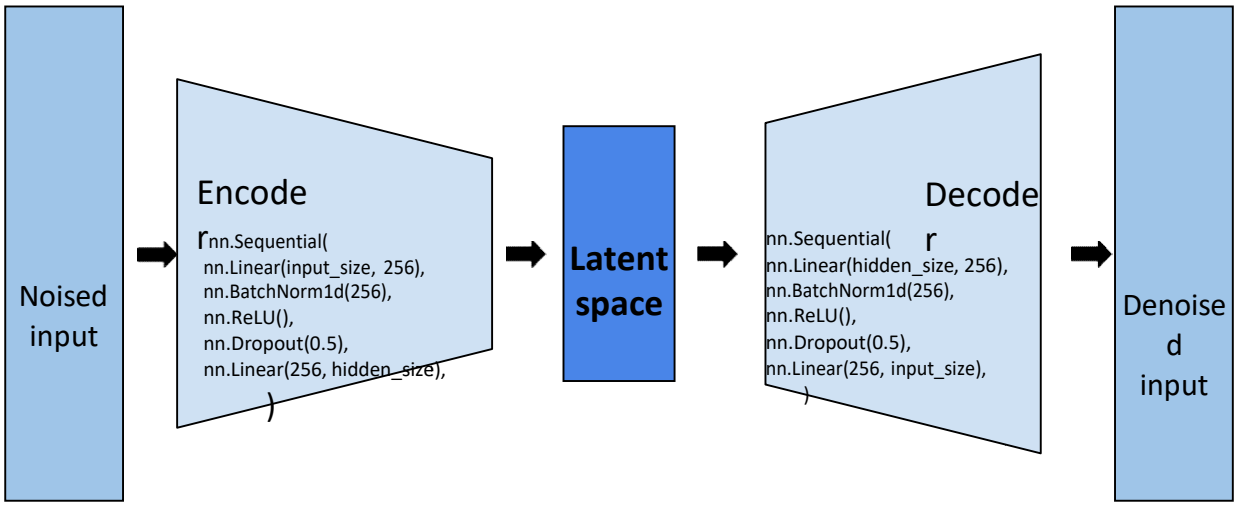

Figure 13:Denoisingautoencoder architecture

Figure 5.8 above highlights the structure used for ourdenoisingautoencoder
Weincludedvariousadvanced techniques and callbacks to our model to ensureits optimal performance and preventitfromoverfitting and learning the noise. One of the techniques weincorporated in ourdenoisingautoencoderisregularisation, in particular, the L1 regularizationwhichisused to preventoverfitting in machine learningmodels. It works by adding a penalty to the costfunction of the model for the L1 norm of the weights. The L1 norm of a vectoris the sum of the absolute values of the elements of the vector.
Wealso fine-tuned the model using the frameworkOptuna and the web solution Weights&Biases (Wandb), bothdiscussed in Chapter 3. Belowis a plot of the training and fine-tuning process of ourdenoisingautoencodershowing multiple trials withdifferent sets of parameters, for example, the blue plot shows a verybad convergence with a lot of fluctuations and oscillations, whichmeansthatthis set of parametersis not good at all and is not up to the expectations of the model's performance, on the other hand, the pink plot alsonoted "best params", demonstrates a very stable convergence to almostreach 0 with no fluctuations, thisindeed shows the stability of the training phase and the ability of the model to learn, the same plot goes to the validation phase, this highlights that the model did not overfit and onlylearn the train data.

ISSN: 2961-6611

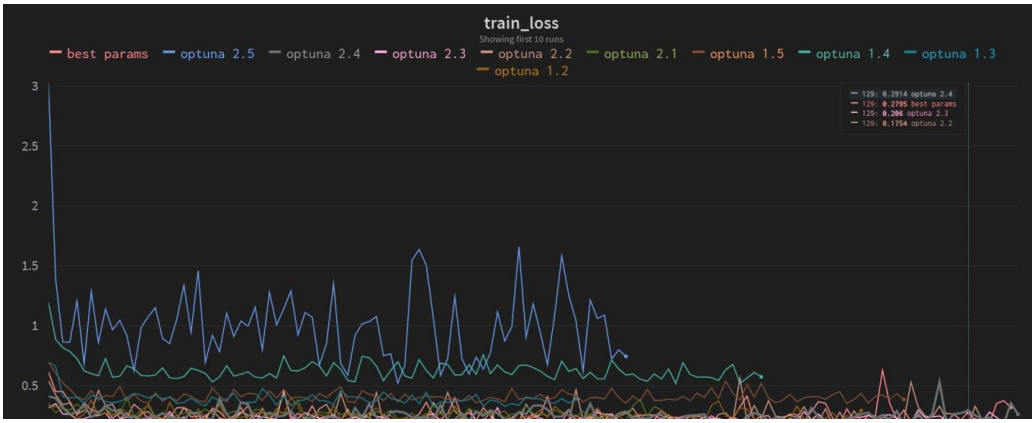

Figure 14:Wandb train loss of variousOptuna runs

Despite the modestresults of the denoisingautoencoder, its extensive runtime was a bottleneck, ittakes up to 14 hours for one train, and in inferenceis not as fast as weneed in order of milliseconds, and given the real-time application of ourproject, time efficiencywas pivotal. As such, our final choiceleanedtowards the Low-Pass and Savitzky-Golay filters, whichprovided the balance betweenaccuracy and expediency.

5-1-Machine learningmodels

Divingfurtherinto the modeling task, beforefullycommitting to deep neural network architectures and complexalgorithms, an exploration intotraditional machine learning algorithmswasdeemednecessary. Thesealgorithms, known for theirprowess in various tasks, offered an alternative perspective on ourgait data. It isalways a good practice to startwithclassic machine learningalgorithms due to theirpowerfulcapabilities, simplicity, and fast training time. In a lot of cases, a simple decisiontree can provide remarkableresults and thusbe the optimal solution[4,5,6].

5-2-Evaluation and comparative study

Afterlisting and discussing the array of models and training techniques to beused, itis time to dive into the training experimentation phase, observe eachmodel's performance, fine-tune it, and establish a comparative study to rankeach model based on precision. We have plottedscatter plots to highlight the actual values versus predictedknee angles of bothLightGBM and XGBoostsinceboth of themprovided the best performances

ISSN: 2961-6611

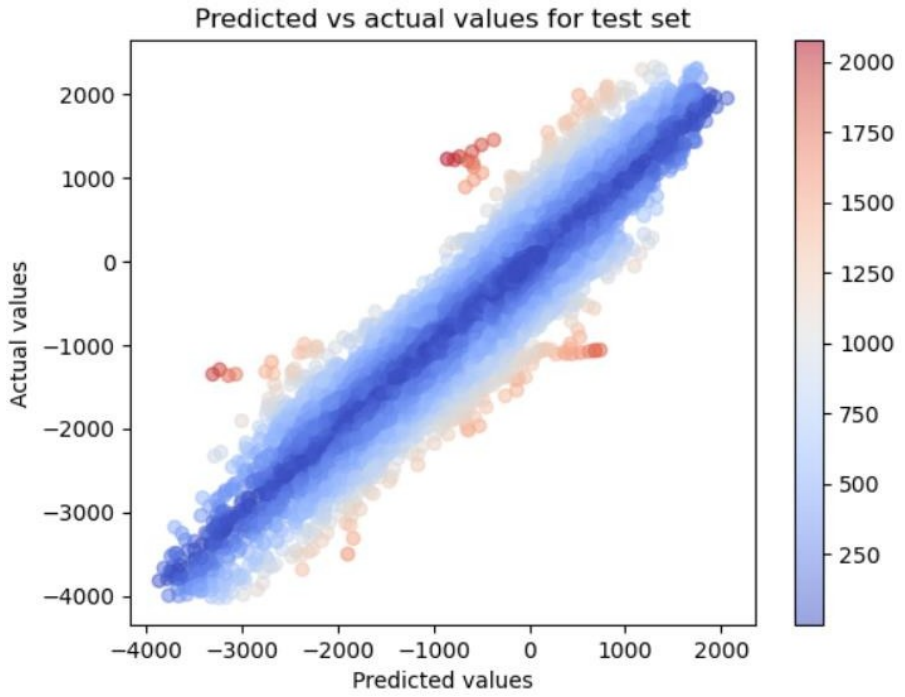

Figure 6.6: Actual vs. predicted values of LightGBM

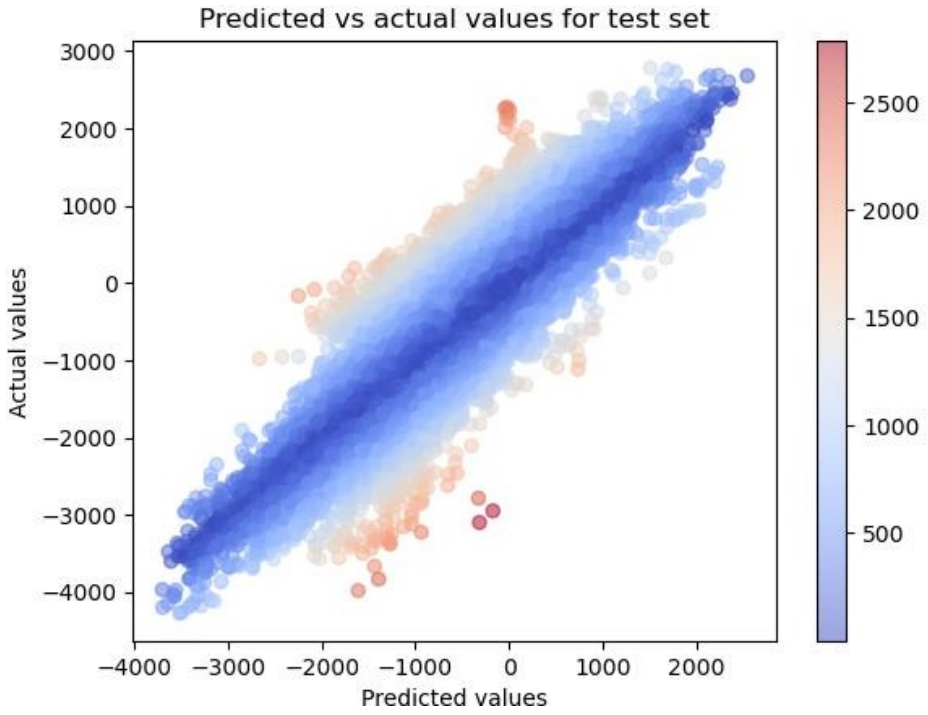

Figure 6.7: Actual vs. predicted values of XGBoost

ISSN: 2961-6611

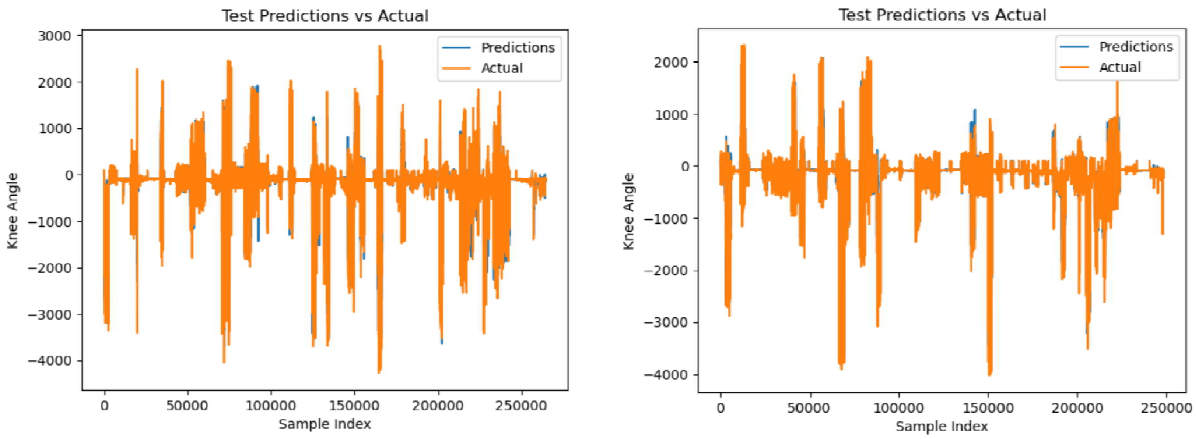

Figure 6.8: Actual vs. predicted values of LGBM on the right and XGB on the left

Based on the scatter plots above, weconcludedthatLightGBMslightlyoutperformedXGBoost in ourregressiontask. Uponfurtheranalysis, here are the results of our comparative studydemonstrated in this table.

Model	Train RMSE	Validation RMSE	Test RMSE	R-squared
Linearregression	55.742	68.896	74.425	0.503
Randomforests regressor	54.254	61.234	70.478	0.538
Support vectorregression (SVR)	49.254	54.236	69.534	0.678
XGBoost	34.784	41.230	40.325	0.775
LightGBMregressor	30.210	34.848	35.264	0.899

Table 1: Comparative study of machine learningmodels

Afterouranalysis, weconclude the choice of LightGBMregressor as ourselected model due to its excellence performance compared to other machine learningmodels. The right question to asknowiswhetherLightGBMisdeployableinsidemicrocontrollers like our Arduino Nano 33 BLE Sense. The short answeris no, and thisis due to manyreasons, first of all, TinyML and embedded AI are still a youngindustry and are stillbeingdeveloped and enhanced. One of the reasonsisalso the compatibility of this model withthesekinds of microcontrollers, as a matter of fact, the LightGBMlibraryisvery large. The Arduino Nano

ISSN: 2961-6611

has limited code space, whichwould not beenough to store the LightGBMlibrary, itisalso a computationallyexpensivealgorithm, on the other hand, the Arduino card has a relatively slow processor, whichwould not be able to run LightGBMefficiently. In order to overcomethischallenge, wechanged the direction of ourresearchtowardsdeeplearningmodelswithspecificframeworksfriendlywithTinyML and embedded AI.

6-Deep learningmodels

Beforedivingintodeeplearningmodels and TinyML compatibility, we have altered the waywefeed the data to models in order to mimic real-life data reception and real-time data reading of time series. First, weneed to understand the amount of data and the length of time seriesneeded to predict one knee angle for the gait cycle, which ranges from 0.98 to 1.07 s, soweneedenough data for every major phase of the locomotion. To do so, wesuggested the implementation of a data generator, whichwillgeneratecontinuoussequencesfromourdataset [4,5,6].

6-1-Models' architectures

Aftercarefulselection of the array of models to betrained, and techniques to beintegratedinto the training process, itismandatory to experimentwith the models' architecture.
Neural network architectures are important becausetheydetermine how the model learns and represents data. The architecture of a neural network consists of the number of layers, the type of layers, the connections between the layers, and the type of activation function.

Experimentingwithdifferent architectures is important becauseit can help us find the best architecture for yourspecifictask. Sometimes a simple architecture can'tlearnenough of complexrelationshipsbetween the features, on the other hand, a complex architecture can lead to overfitting, thuspoor performance in both cases.

One of the restrictions whenitcomes to architectures of neural networks used in ourresearchis the limitedability to experimentwithcomplex and large architectures. The reason for thisis the limitedcomputationalresources of microcontrollerssuch as our Arduino Nano 33 BLE Sense. As a matter of fact, even simple neural networks can have a large number of parameterswhichmakesitalmost impossible to deploythemintotheseboards.
Belowis a table demonstrating the architectures used for each type of neural network:

ISSN: 2961-6611

Model	Architecture 1	Architecture 2	Architecture 3	Architecture 4	Architecture 5
LSTM	3 layers (128-64-32) units - OL	3 layers (64-32-16) units - OL	2 layers (64-32)units - OL	2 layers (32-16) units - OL	2 layers (16-8) units - OL
GRU	3 layers (128-64-32) units - OL	3 layers (64-32-16) units - OL	2 layers (64-32)units - OL	2 layers (32-16) units - OL	2 layers (16-8) units - OL
CNN	2 1D layers (128-256) units - OL	2 1D layers (64-128) units - OL	2 1D layers (32-64) units - OL	2 1D layers (16-32) units - OL	2 1D layers (8-16) units - OL
CNN-LSTM	1D layer (128-256) units- LSTM layer 64 units - OL	1D layer (64-128) units- LSTM layer 32 units - OL	1D layer (32-64) units- LSTM layer 32 units - OL	1D layer (16-32) units- LSTM layer 32 units - OL	1D layer (8-16) units- LSTM layer 16 units - OL
CNN-GRU	1D layer (128-256) units- GRU layer 64 units - OL	1D layer (64-128) units- GRU layer 32 units - OL	1D layer (32-64) units- GRU layer 32 units - OL	1D layer (16-32) units- GRU layer 32 units - OL	1D layer (8-16) units- GRU layer 16 units - OL

Table 6.5: Learning rate schedulers

In each architecture mentioned in the table above, weexperimentedwith and without batch normalization and dropout layers.

Batch normalization:is a technique used to normalize the inputs of each layer in a neural network. This helps to improve the training process and to make the model more robust to noise in the data.

Dropout layer:is a regularization technique used in neural networks to preventoverfitting. It works by randomlydropping out unitsfrom the network during training. This forces the network to learn to rely on multiple units to makepredictions.

6.2.4 Evaluation and comparative study

Aftercareful training of ourdeeplearningmodelswithdifferent architectures, incorporating the mostpractical techniques in the data science realm, this process tookfrom 6 to 14 hours of training for each model, wegotmodestresults, not up to ourexpectations, but still a hugemilestone in ourresearch. This is due to the limitedability to experimentwith more complex architectures because of the poorcomputational power of ourmicrocontroller,

ISSN: 2961-6611

eventhoughourmodels are robust, theyweren't able to minimize the error to a minimal degreerangingfrom 1 to 5 degrees.

Belowis the table summarizing the best results of each neural network with the best architecture.

Model	Architecture	MAE
LSTM	2 layers (64-32)units - OL	32
GRU	2 layers (32-16) units - OL	23
CNN	2 1D layers (64-128) units - OL	20
CNN-LSTM	1D layer (16-32) units- LSTM layer 32 units - OL	31
CNN-GRU	1D layer (32-64) units- GRU layer 32 units - OL	21

Conclusion :

In summary, ourresearchculminatedwith a thorough discussion of methods and techniques aimed at improvingouroutcomesthrough updates to both data collection protocols and the hardware integratedinto the bionic leg. Uponreflection, thisendeavorencapsulated the essence of a scientificinquiryjourney. It encompassed the entirespectrum, fromcomprehending the intricacies of the problem to meticulous data preparation, fromexperimentingwithvariousmodels to successfullypredicting the target variable. Eachstepserved as a valuablelesson in fostering innovation and mastering the delicate balance betweentheoretical concepts and practical application.

ISSN: 2961-6611

References :

[1] Chereshnev R., Kertész-Farkas A. (2018) HuGaDB: Human GaitDatabase for Activity Recognition fromWearableInertialSensor Networks. In: van der Aalst W. et al. (eds) Analysis of Images, Social Networks and Texts. AIST 2017. Lecture Notes in Computer Science, vol 10716. Springer, Cham

[2] Zomar, B.O.; Bryant, D.; Hunter, S.; Howard, J.L.; Vasarhelyi, E.M.; Lanting, B.A. A randomised trial comparingspatio-temporalgaitparametersafter total hip arthroplastybetween the direct anterior and direct lateralsurgicalapproaches. HIP Int. 2018, 28, 478–484.

[3] Sprager, Sebastijan, and MatjazJuric. "Inertialsensor-basedgaitrecognition:areview." Sensors 15.9 (2015): 22089–22127.

[4] Teufl, Wolfgang, et al. "TowardsInertialSensorBased Mobile GaitAnalysis: Event-Detection and Spatio-TemporalParameters." Sensors 19.1 (2019): 38.

[5] Delgado-Escaño, Rubén, et al. "An End-to-End Multi-Task and Fusion CNN for Inertial-BasedGait Recognition." IEEE Access 7 (2019): 1897–1908.

[6] Sainath, Tara N., et al. "Convolutional, long short-term memory, fullyconnecteddeep neural networks." 2015 IEEE International Conference on Acoustics, Speech and Signal Processing (ICASSP). IEEE, 2015.

[7] Ngo, Thanh Trung, et al. "The largestinertialsensor-basedgaitdatabase and performance evaluation of gait-basedpersonalauthentication." Pattern Recognition 47.1 (2014): 228–237.

[8] Hung, Tran, and Young Suh. "Inertialsensor-basedtwofeet motion tracking for gaitanalysis." Sensors 13.5 (2013): 5614–5629.

[9] Dehzangi, Omid, MojtabaTaherisadr, and RaghvendarChangalVala. "IMU-basedgait recognition usingconvolutional neural networks and multi-sensor fusion." Sensors 17.12 (2017): 2735.

[10] Caldas, Rafael, et al. "A systematicreview of gaitanalysismethodsbased on inertialsensors and adaptive algorithms." Gait& posture 57 (2017): 204–210.

[11] Zeni Jr, J. A., J. G. Richards, and J. S. Higginson. "Two simple methods for determininggaiteventsduringtreadmill and overgroundwalkingusingkinematic data." Gait& posture 27.4 (2008): 710–714.

ISSN: 2961-6611

Progress in Renewable Energy Integration and Power System Stability using GFL and GFM Inverters

Mohamed Elleuch, Khadija Ben Kilani

University of Tunis El Manar, ENIT-LSE, LR11ES15,
B.P 37 Le Belvédère, 1002 Tunis, Tunisia
Mohamed.elleuch@enit.utm.tn
Khadija.kilani@enit.utm.tn

***Abstract*— This paper deals with the evolution and applications of advanced inverter-based resources (IBR) in electric power networks. It highlights the transition from grid-following (GFL) inverters to grid-forming (GFM) inverters, emphasizing the importance of addressing concerns with IBRs to facilitate the integration of renewable energy generation. Various examples of inverter operating modes and applications in renewable energies integration, microgrid and larger HVDC transmission grids have been tested. It also focus on inverter control modes, for grid code requirement (GCR) in terms of Voltage ride through (VRT) and Frequency ride through (FRT) as well as power system stabilization. The results shown through this paper underscores the significance of transitioning more inverters from GFL to GFM modes to ensure grid stability as Inverter Based Resources (IBR) from renewable energies penetration increases.**

***Keywords*— Renewable energies integration, inverter-based resources (IBR), grid-following (GFL) inverters, grid-forming (GFM) inverters, grid code requirement (GCR) .**

I. INTRODUCTION

The Figure 1 shows many systems that use power electronics (inverters) to interface with the grid [1]. Various technologies of these inverters have been used to integrate renewables energies into the grid. Obviously, wind energy and photovoltaic (PV) are the most widely used renewable energy sources, leading to High Penetrations of Inverter-Based Resources (IBRs) into the electrical network [2].

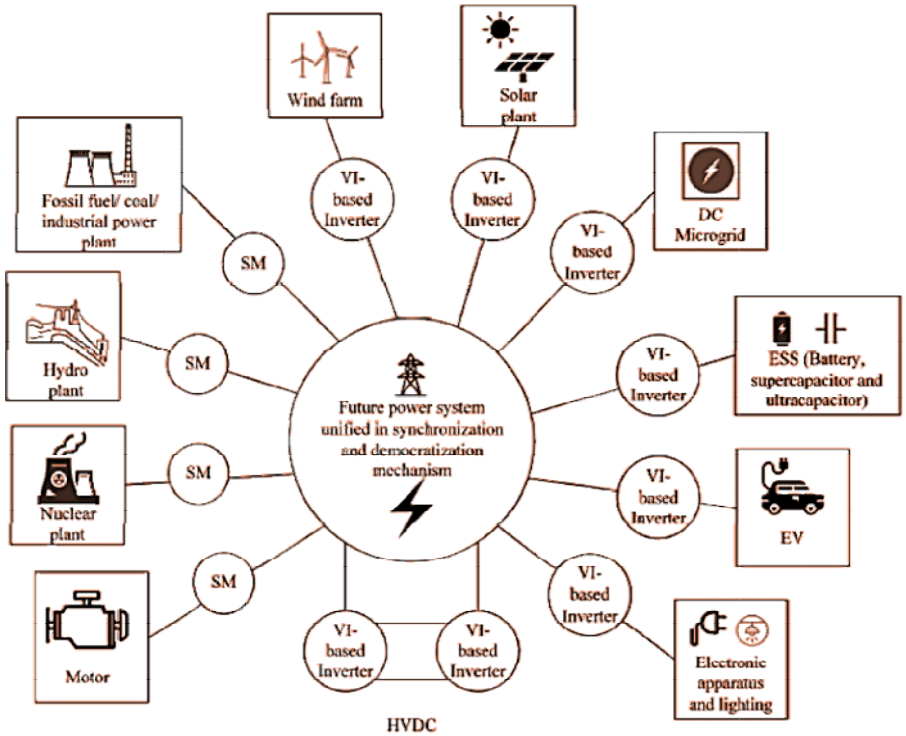

Fig.1- The application of conventional Synchronous Machines (SM) and Voltage/Current (VI) Based Inverter

ISSN: 2961-6611

As the integration rate of renewable energies evolves, the synchronous machines that traditionally provide the system services required for stable grid operation are being replaced by inverter-based resources (IBRs), such as wind power, solar photovoltaics and battery storage. With the increasing proliferation of IBRs, some synchronous areas will operate with high IBR penetrations, making it essential that IBRs become an essential support to ensure grid stability.

Inverters in service today are predominantly "grid following" (GFL), with characteristics different from synchronous generators. However, "grid-forming" (GFM) inverters are being developed and becoming commercially available. They can be designed to satisfy the essential system needs that synchronous machines fulfill. Many services are possible for both inverters and synchronous machines to deliver, including voltage, frequency, and stability support (Fig.2)[3].

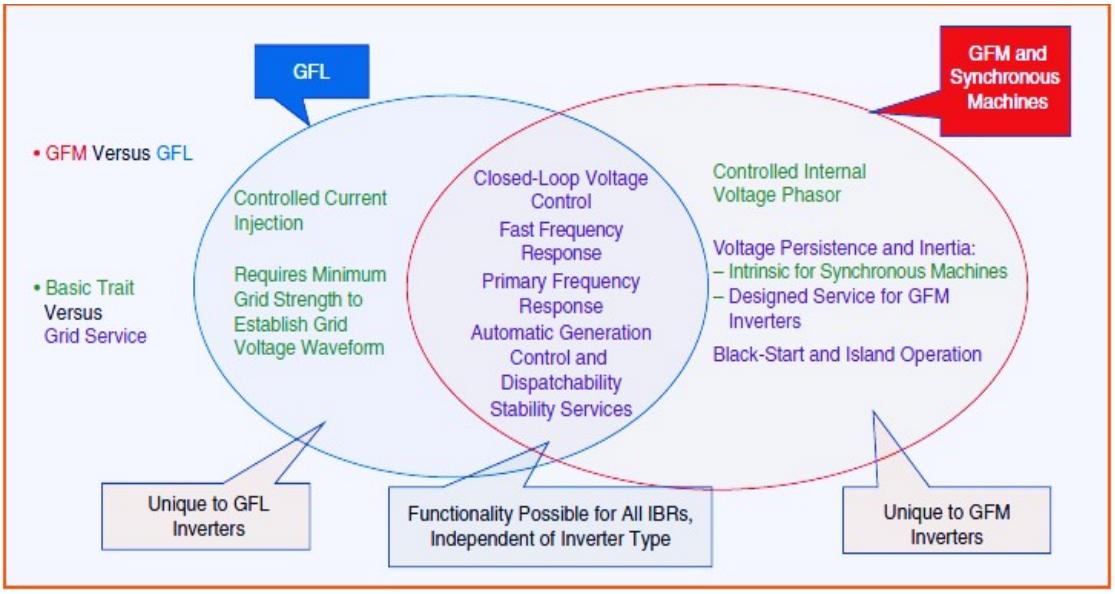

Fig.2-features and grid services of GFL IBRs , GFM IBRs and Synchronous Machines [3]

In addition, various applications of inverters in HVDC links have been evolved for enhancing the stability and reliability of power electronic systems, particularly in the context of high renewable energy integration (off shore wind plant and longer transmission lines) and the need for grid modernization [4]

II. High Penetrations Challenges of (IBRs) on Power Systems

Increasing penetration of IBRs (e.g., wind, solar, HVDC) is transforming power systems. high level penetration of IBRs presents several operational challenges as:[5]

- Reduction in system inertia leading to higher rate of change of frequency (RoCoF) and larger frequency deviations
- Reduction in transient stability margins and controllable reactive power resources
- Voltage dip-induced frequency events in electrically smaller power systems
- Increased need for real-time energy balancing due to renewable forecast errors
- Observability and controllability issues with IBRs
- Reduction in short-circuit levels affecting protection schemes and power quality
- Emergence of new forms of instability driven by IBR control interactions

New strengths must be found from IBRs to address the challenges posed on grid stability involving advanced Inverters to support the systems. Recent research has focused on grid forming (GFM) technologies, which are proving to be advantageous compared to the older grid following (GFL) inverters under certain operating conditions.

ISSN: 2961-6611

An easy way to comply with the conference paper formatting requirements is to use this document as a template and simply type your text into it.

A. GFM versus GFL

The reduction of system services provided by synchronous generators weakens the grid and may lead to stability concerns, particularly in low-system-strength conditions and high rates of change of frequency (RoCoF) after contingencies [5]. Figure 3 shows the control principle diagram for each IBRs Controls and Table 1 summarizes the characteristics of the GFL inverter versus the GFM one [6-7].

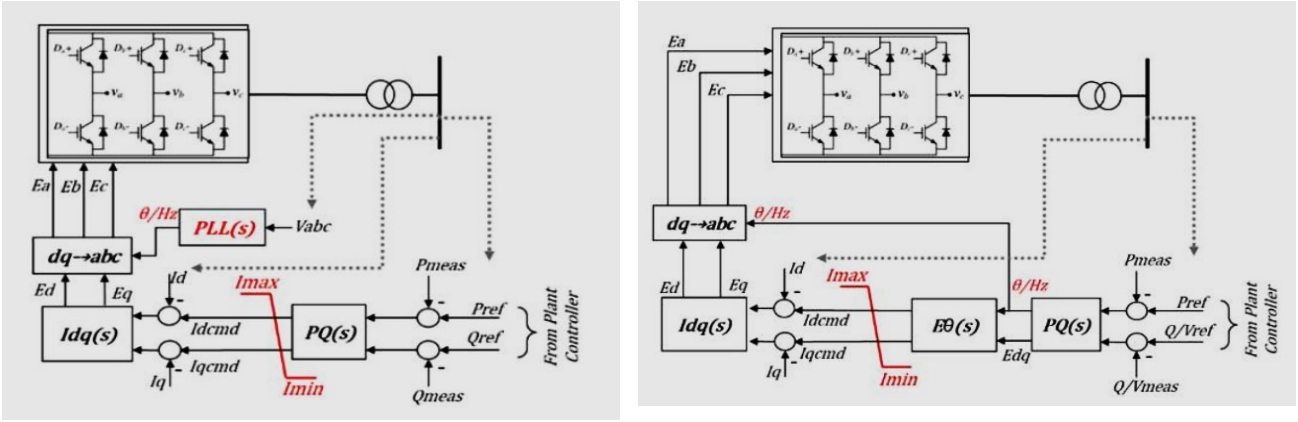

Fig. 3. Block diagram control of
a) GFL inverter b) GFM inverter

Table 1
COMPARISON BETWEEN THE GRID-FORMING INVERTER (GFM) AND THE GRID-FOLLOWING INVERTER (GFL)

Features	Grid-Forming Inverter (GFM)	Grid-Following Inverter (GFL)
Control	Can operate in standalone mode and act as a virtual synchronous generator (VSG). Can control the voltage and frequency of the entire system.	Follows the grid's voltage and frequency and maintains a constant power output in synchronization with the grid.
Ancillary Services	Can provide primary frequency control, secondary frequency control, and inertial response, which are essential for the stability of the power system.	Can only provide reactive power control and voltage control as ancillary services.
Frequency and Voltage Ride Through	Has better frequency and voltage ride through capabilities than GFL. Can adjust its output power in response to a change in frequency and voltage.	Can only follow the grid's voltage and frequency. Cannot adjust its power output in response to a change in frequency or voltage.
System Stability	Suitable for standalone systems where grid stability is crucial. Can maintain system stability in the absence of the grid.	Suitable for systems that are already connected to the grid and need to follow the grid's voltage and frequency. Cannot maintain system stability in the absence of the grid.
Response Time	Faster response to changes in load and grid conditions	Relatively slower response to changes in the grid
Power Quality	Provides high power quality due to its ability to control voltage and frequency.	May not provide high power quality, as it is designed to follow the grid's voltage and frequency.
black start capability	providing black start support for power system restoration after a major outage	not possible
Inverter Cost	Higher inverter cost due to additional hardware and software required for VSG operation. the cost of a 250 kW GFM inverter can range from $50,000 to $100,000 or more, depending on the manufacturer and features.	Lower inverter cost due to simpler hardware and software requirements. 250 kW GFL inverter can cost between $20,000 to $40,000, depending on the manufacturer and features
Applications	• Standalone microgrids • Islanded renewable energy systems • Hybrid power systems with high penetration of renewable energy sources • Remote power systems with limited access to the grid	• Grid-tied renewable energy systems • Energy storage systems • Electric vehicle charging stations • Distributed energy resources in residential and commercial buildings

ISSN: 2961-6611

B. Other Mitigation Options

<Mitigation options have been adopted such as installing Synchronous Condenser (SynCons), maintaining inertia from synchronous machines, control tuning, coordination, and improving power system modeling and simulation tools [1]. These options can address stability concerns but may also introduce new challenges. In addition, The definition of a new grid code and standards should enable the integration of large-scale RES into the power grid, by enforcing IBR emulation [8]. The frequency regulation should be contributed by RES, and grid-forming inverter should be mandatory (Fig.4).

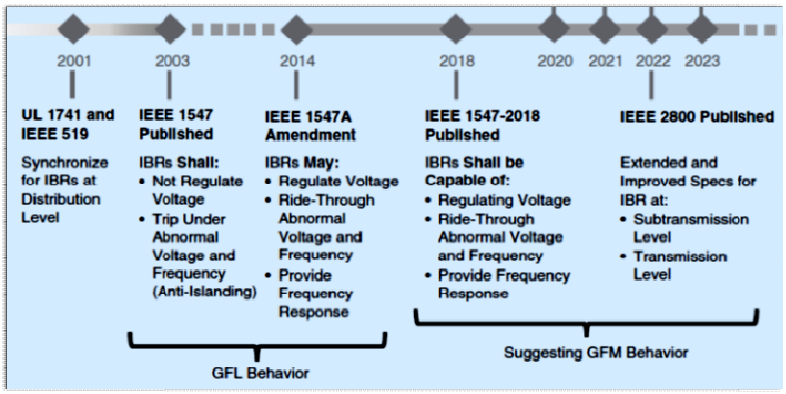

Fig. 4 Evolution of regulatory landscape for IBRs as qualified by relevant standards [9]

III. CASE STUDIES

A. PV and Wind energies integration under GCR [10]

The study proposes an improved control scheme for the integration of variable-speed wind generators and solar photovoltaic systems into the power grid (Fig.5). The control strategy based on the synchronverter technology (GFM), applied to the gridside converter for the connection of wind and photovoltaic systems. The parameters of the converter regulator are tuned based on a specific residue's method. The proposed control performances were evaluated in comparison with the conventional GFL voltage-oriented control (VOC) in term of accordance with Grid Code Requirements (GCR).

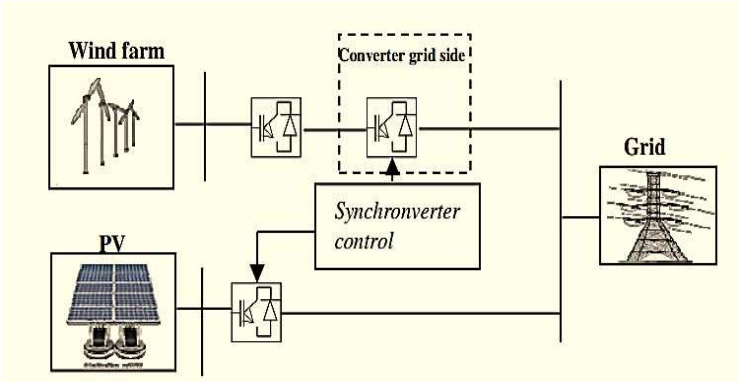

Fig. 5. Inverters used in PV/Wind integration system.

1) PV Results:

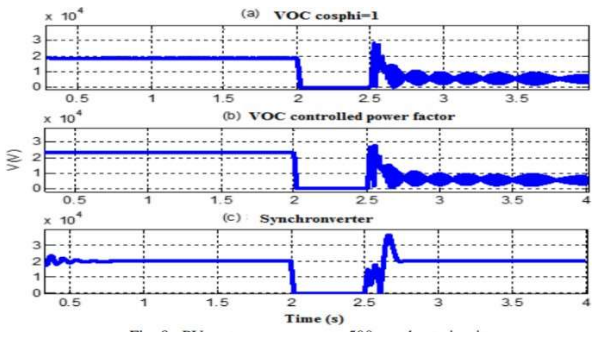

Fig.6 . PV Voltage Ride Through with GFL/GFM

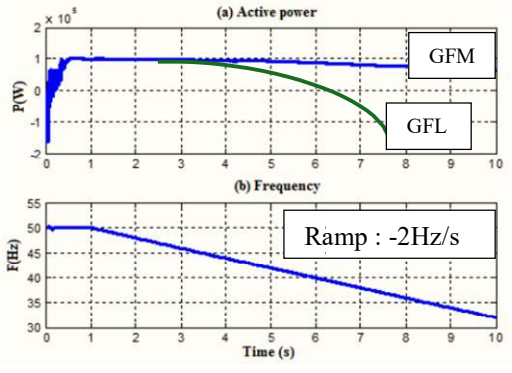

Fig.7. PV Frequency Ride through with GFM/GFL Control

ISSN: 2961-6611

Dynamic performances tested include low voltage ride through, frequency ride through, and fault critical clearing time. The results show that the GFM control ensures better performances, complies with the GCR of the power system operator and enhances the grid stability (Fig.6-7).

2) Wind Plant Ancillary services results [11]

GFM Inverter control strategies have been developed for wind power plants (Fig.8) to meet recent grid code requirements and ancillary services (Fig.9). These controls allowed the wind farm to participate in system ancillary services as provided by conventional power plants. Hierarchically, priority is given to the centralized control.

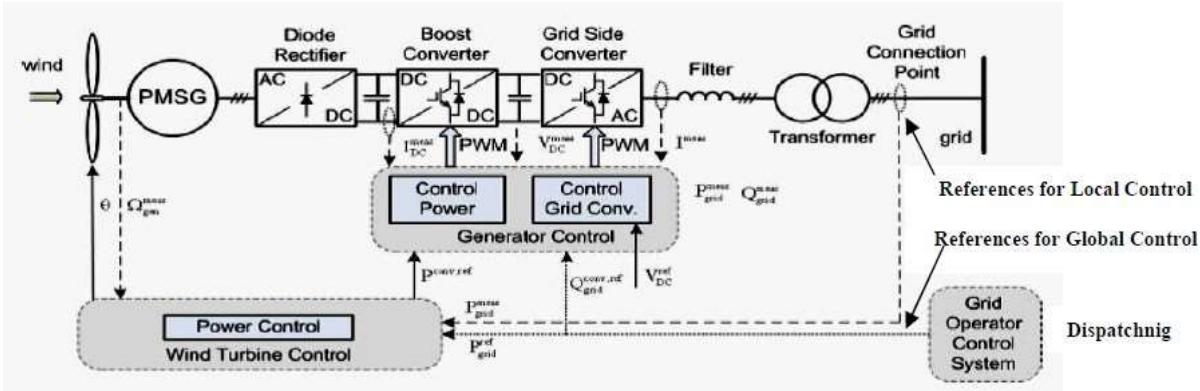

Fig.8. GFM control in Wind plant: Local control according to PoC references; Centralized control from the dispatching

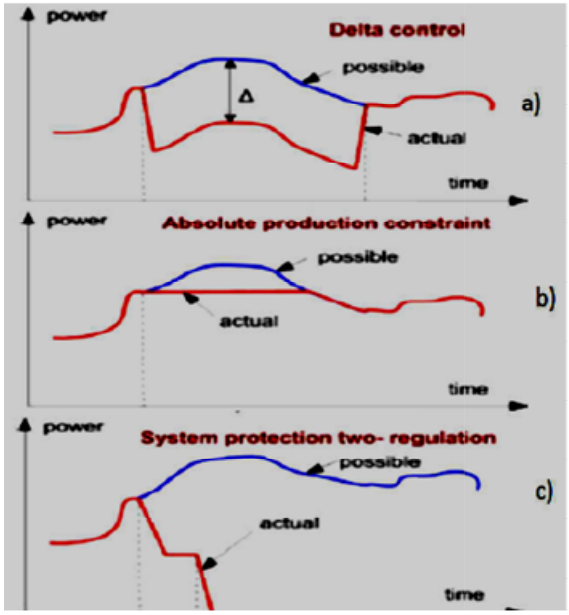

Fig.9. Active power control implemented in wind farm to comply with recent GCR

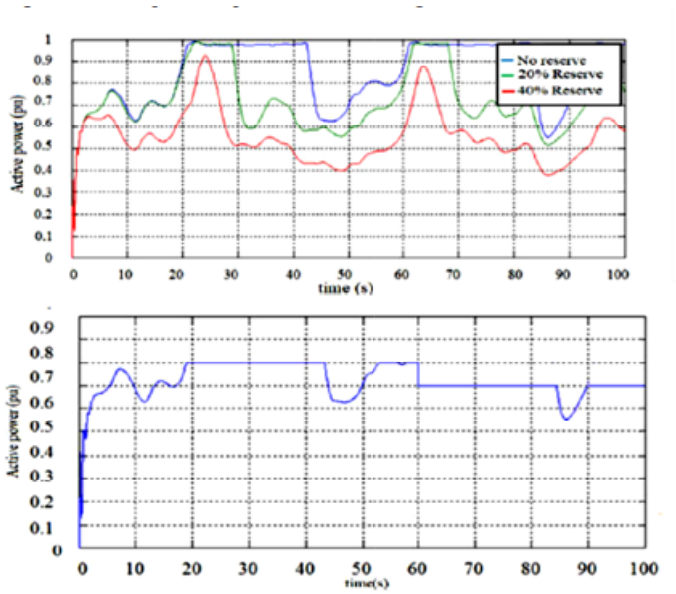

Fig.10. Wind farm active power output under:
a) Delta Control; b) Absolute production constraint

These controls have been tested to operate the wind power plant with power reserve or with curtailment (Fig.10). Similarly, the emergency shutdown of the wind power plant was tested, following the instruction of the network operator, while respecting the ramp-down rates required by the Grid Code**.**

B. IBRs in HVDC

1)IEEE 9 Bus Results

The IEEE 9-bus power system, shown in Fig.11, is modified by The replacement of line 4-5 by an HVDC transmission line. The HVDC link is 100 km long, has a rated power of 200 MW and a DC voltage rating of ±100 kV (Fig. 11). The comparison between GFM (SVC Technology) and GFL (LCC technology) confirms the improvement of the grid stability in favor of GFM control as shown in (Fig.12) and table 2. It's obvious that LCC

ISSN: 2961-6611

converters used for GFL operation provide high power transmission capabilities but have limitations in terms of independent control of active and reactive power compared to VSC converters.

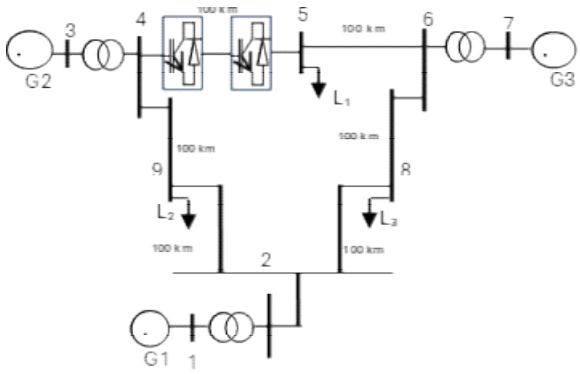

Fig.11. Modified IEEE 9 bus system

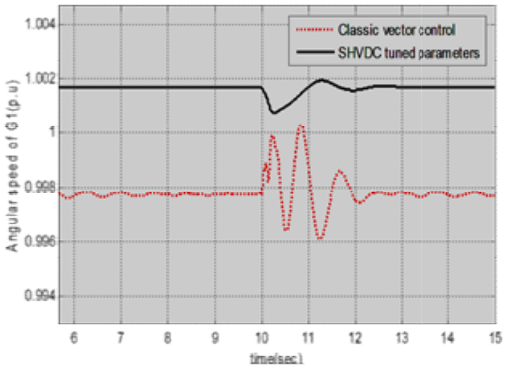

Fig.12. Responses of the angular speed to a 100 ms short circuit near to G2 : Angular speed of G1 (p.u)

Table 2
CRITICAL CLEARING TIMES WITH BOTH CONTROL STRATEGIES

CCT (ms)	G1	G2	G3
GFM control	250	200	200
GFL control	150	120	150

2) HVDC Interconnexion Ancillary Services

Recent VSC-HVDC interconnections (Voltage Source Converter) based on GFM control mode, have been chosen to enable providing ancillary services [12], including primary and secondary frequency control, inertial response, voltage support, and black start capability for power system restoration after a major outage [13] (Table 3**).** Figure 13 shows the Tunisia -Italy interconnexion model used for testing stability (Fig. 14) and other ancillary services under GFL (LCC) and GFM (SVC) HVDC interconnexion control.

Table 3
EXAMPLES OF SVC-HVDC (GFM) INTERCONNEXION,
PROVIDING PRIMARY AND SECONDARY FREQUENCY CONTROL, REACTIVE POWER SUPPORT

Interconnection	Capacity	Technology	Configuration	Cable Length	Operational Year
NordLink Norway - Germany	1.4 GW	SVC-HVDC	Bipole	623 km	2021
Viking Link **UK - Denmark**	1.4 GW	SVC-HVDC	Bipole	760 km	2023
COBRAcable **Netherlands - Denmark**	700 MW	SVC-HVDC	Bipole	325 km	2019
Tunisia-Italy	600 MW	SVC-HVDC	Bipole	200 km	2028 ?

ISSN: 2961-6611

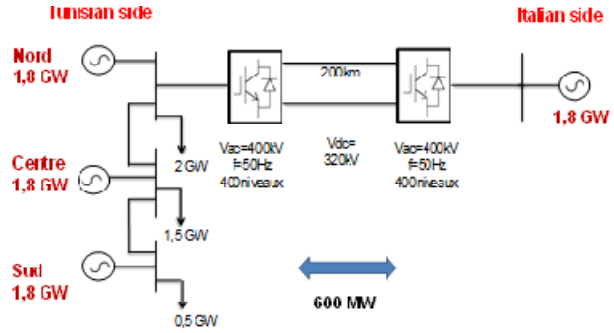

Fig. 13. HVDC interconnexion Mode: between Tunisia and Italy

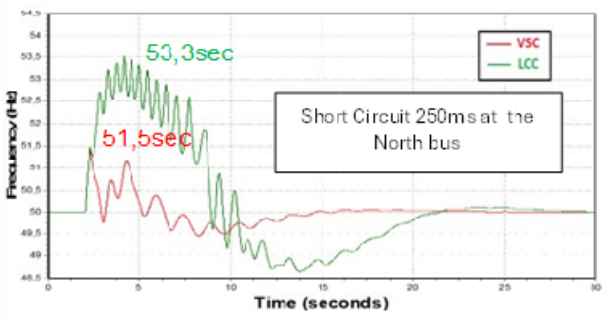

Fig. 14 frequency in Tunisa side following short circuit with GFM or GFL control of the interconnexion converter

3) Islanded MicroGrid: BESS under GFL or GFM control

To address stability concerns, Synchronous Condenser (SynCons) have been used to maintain inertia from synchronous machines. In the Micro-grid shown in Fig.15, The lack of inertia have been tested when removing the SynCons under GFMLGFL control of the Batteries Electrical Storage Systems (BESS). Simulation results (Fig.16) confirm that only under GFM control where the micro-grid stability could withstand the lack of Synchronous inertia [14].

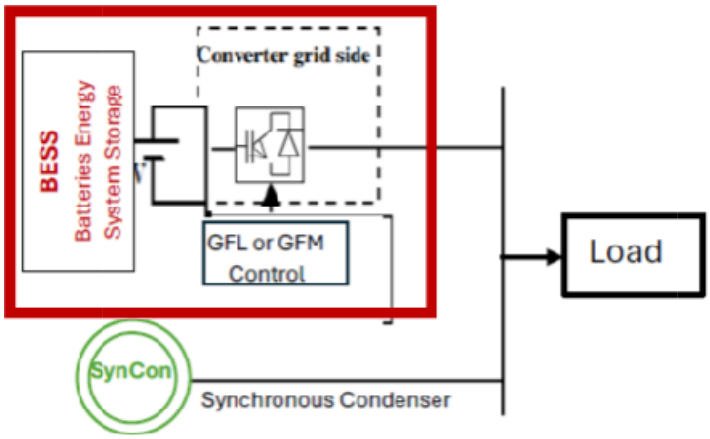

Fig. 15. Microgrid configuration: BESS (2.2MW) under GFL or GFM control with or without SynCon (2.5 MVA) [15]

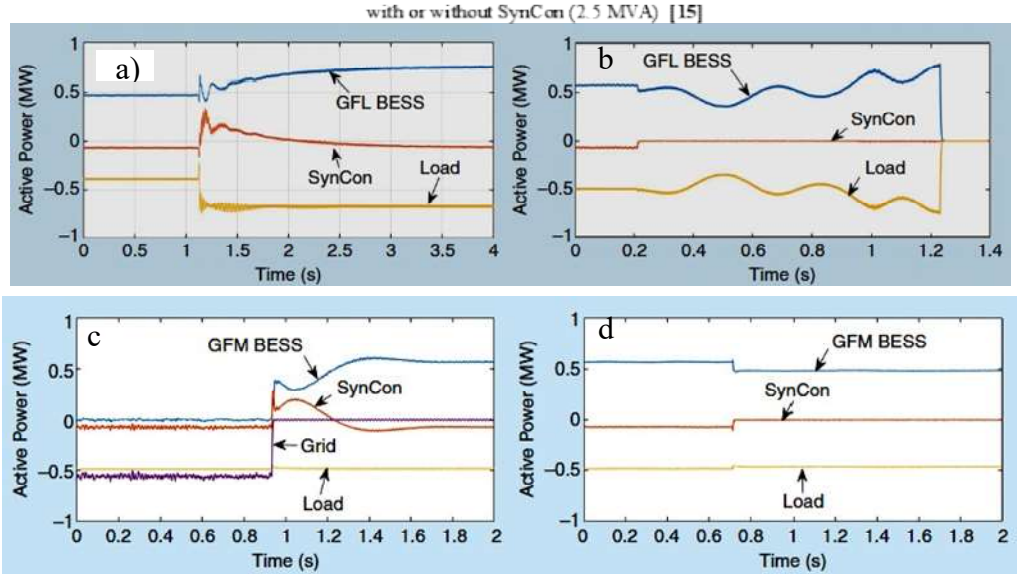

Fig.16- MicroGrid operation on islanded mode [15]
a)GFL control with SynCon- b)GFL Control with SynCon tripping c)GFM control with SynCon: d) GFM control

ISSN: 2961-6611

IV. CONCLUSION

The choice of inverter technology for connecting renewable energy sources to the grid or to build HVDC interconnexion depends on several factors as the grid code requirements, and specific needs of the power system. Grid-following (GFL) inverters are commonly used for connecting PV plants and wind farms to the grid with limited capabilities for maintaining grid stability and power quality. In contrast, grid-forming (GFM) inverters are gaining attention for large-scale renewable energy systems as well as for micro-grids where they can operate in islanded mode. They are well-suited for high rate of renewable energy systems integration into the grid, as they can provide primary frequency control, secondary frequency control, and inertial response, which are essential for the stability of the power system.

The future trend is towards increased use of GFM inverters, driven by the need to integrate large-scale renewable energy systems into the grid while maintaining grid stability. The cost of GFM inverters has been decreasing, and their performance and reliability have been improving; but may lead to new issues such as ; Observability and controllability with IBRs, Reduction in short-circuit levels affecting protection schemes and power quality, Emergence of new forms of instability driven by IBR control interactions [15].

REFERENCES

[1] Kah Yung Yap and all, *Virtual Inertia-Based Inverters for Mitigating Frequency Instability in Grid-Connected Renewable Energy System: A Review*, Applied Science Journal: December 2019.

[2] Leo Casey, and all , *Advanced Inverter Interactions With Electric Grids*, IEEE power electronics magazine, pp.20-27, June 2023.

[3] Julia Matevosyan,Jason, and al, *A Future With Inverter-Based Resources Finding Strength From Traditional Weakness*, IEEE power & energy magazine, november/december pp.18-28, 2021.

[4] Karimi, H., & Davari, M.. *Damping of Low-Frequency Oscillations in Power Systems Using VSC-HVDC Transmission Systems*. IEEE Transactions on Power Systems, 36(4), 3422-3433, 2021.

[5] Nilesh Modi , and all, "*High Inverter-Based Resource Integration The Experience of Five System Operators",* IEEE power & energy magazine, pp.78-88, march/april 2024.

[6] Alassi, A., Mehdi, S., Azeez, N. A., & Farrell, M. *Grid-Forming Inverters: A Review of Contributing Elements Towards Successful Grid Integration.* IEEE Access, 9, 29223-29243. 2021.

[7] Baumann, M., Jauch, C., & Ackva, A., *Comparison of Grid-Forming and Grid-Following Inverter Control Strategies for Renewable Energy Systems*. Energies, 16(3), 1088, 2023.

[8] Behrooz Bahrani and al , *"Grid-Forming Inverter-Based Resource Research Landscape",* IEEE power & energy magazine, pp.80-88, March/April 2024.

[9] *IEEE Standard for Interconnection and Interoperability of Inverter-Based Resources Interconnecting With Associated Transmission Systems*, IEEE Standard 2800-2022, Feb. 2022.

[10] Raouia Aouini, Ichrak Nefzi, Khadija Ben Kilani, Mohamed Elleuch, *Exploitation of Synchronverter Control to Improve the Integration of Renewable ; VSources to the Grid,* J. Electrical Systems 13-3- 543-557, 2017.

[11] Imen Karray, Khadija Ben Kilani, Mohamed Elleuch, *Wind Plant Control Under Grid Code Requirements*, 16th International Multi-Conference on Systems, Signals & Devices (SSD'19), Turkey 2019

[12] I. Karray , K. Ben Kilani, M. Elleuch *Progress of HVDC interconnections and case study,* ICRAES-2019 December, 23-25, Hammamet, Tunisia 2019.

[13] Xu, Z., Liu, Y., Zhou, W., & Zheng, S., *Black start strategy of VSC-HVDC system based on multi-agent reinforcement learning.*, IET Generation, Transmission & Distribution, 15(6), 797-805, 2021.

[14] Nilesh Modi and all, *"High Inverter-Based Resource Integration The Experience of Five System Operators",* IEEE power & energy magazine, pp.78-88, march/april 2024.

[15] Babak Badrzadeh , Carmen Cardozo and al. *Grid-Forming Inverters, Project Demonstrations and Pilots,* IEEE power & energy magazine, pp.66-77, March/April 2024.

ISSN: 2961-6611